Received: 15 January 2024 | Revised: 31 August 2024 | Accepted: 13 September 2024

IET Generation, Transmission & Distribution

DOI: 10.1049/gtd2.13279

The Institution of Engineering and Technology WILEY

ORIGINAL RESEARCH

Parameter identification of PV solar cells and modules using bio dynamics grasshopper optimization algorithm

Mostafa Jabari[1] | **Amin Rad**[1] | **Morteza Azimi Nasab**[2] | **Mohammad Zand**[2] | **Sanjeevikumar Padmanaban**[2] | **S. M. Muyeen**[3] | **Josep M. Guerrero**[4,5]

[1]Faculty of Electrical Engineering, Sahand University of Technology, Tabriz, Iran

[2]Department of Electrical Engineering, Information Technology and Cybernetic, University of South-Eastern Norway, Porsgrunn, Norway

[3]Department of Electrical Engineering, Qatar University, Doha, Qatar

[4]Center for Research on Microgrids, University of Aalborg, Aalborg, Denmark

[5]Center for Research on Microgrids (CROM), Department of Electronic Engineering, Technical University of Catalonia, Barcelona, Spain

Correspondence
S. M. Muyeen, Department of Electrical Engineering, Qatar University, Doha, Qatar.
Email: sm.muyeen@qu.edu.qa

Abstract

The escalating global population and energy demands underscore the critical role of renewable energy sources, particularly solar power, in mitigating environmental degradation caused by traditional fossil fuels. This paper emphasizes the advantages of solar energy, especially photovoltaic (PV) systems, which have become pivotal in hybrid energy systems. However, accurate modelling and identification of PV cell parameters pose challenges, prompting the adoption of meta-heuristic optimization algorithms. This work explores the limitations of existing algorithms and introduces a novel approach, the bio-dynamics grasshopper optimization algorithm (BDGOA). The BDGOA addresses deficiencies in both exploration and exploitation phases, exhibiting exceptional convergence speed and efficiency. The algorithm's simplicity, achieved through the implementation of an elimination phase and controlled search space, enhances its performance without intricate calculations. The study evaluates the BDGOA by applying it to identify unknown parameters of five solar modules. The algorithm's effectiveness is demonstrated through the extraction of parameters for RTC France, PWP201, SM55, KC200GT, and SW255 models, validated against experimental data under diverse conditions. The paper concludes with insights into the impact of radiation and temperature on module parameters. The subsequent sections of the paper delve into the intricacies of the PV cell and module model, articulate the formulation of the proposed algorithm, present simulations, and analyse the obtained results. The BDGOA emerges as a promising solution, overcoming the limitations of existing algorithms and contributing significantly to the advancement of accurate and efficient PV cell parameter identification, thereby propelling progress towards a sustainable energy future.

1 | INTRODUCTION

Nowadays, owing to the exponential rise in global population and the escalating demands for energy, the significance of renewable energy sources, especially solar power, should be emphasized sufficiently. The advantages offered by renewable energy technologies are particularly evident when compared to traditional fossil fuels. Although fossil fuels have gained popularity due to their high efficiency and widespread utilization, they come with severe detrimental effects on the environment, such as pollution, depletion of the ozone layer, emissions, global warming, and climate change [1, 2]. Growing concerns regarding the impact of global warming and pollution have instigated a shift away from limited and environmentally harmful fossil fuels. Consequently, there has been a global impetus to incorporate renewable energy sources like wave, tidal, wind, and geothermal power generation into electricity networks to meet the ever-increasing demand for energy in recent decades [3–5]. The quest for viable solutions to combat environmental degradation and the limited availability of non-renewable resources has led to the emergence of renewable energy alternatives as an indispensable solution. Renowned for their ability to generate energy with minimal environmental consequences, renewable energy sources, particularly solar power, have gained significant

momentum and are being extensively harnessed in numerous countries worldwide [1].

Solar energy has emerged as a top choice for hybrid energy systems due to its minimal environmental impacts; low pollution, and wide accessibility. It offers various advantages such as efficiency, ease of installation, low emissions, and compatibility with technologies like hydrogen production, battery storage, and diesel power systems [6–8]. Among solar energy technologies, photovoltaic (PV) systems are particularly advantageous. They enable straightforward installation, require minimal maintenance, offer an essentially limitless energy supply, operate silently, and provide flexibility in system size. As a result, PV systems rank as the world's second-most environmentally friendly energy source after wind energy systems [9, 10]. However, to achieve optimal performance, it is crucial to accurately model and identify parameters for PV systems. This includes the precise identification of PV cell and module parameters, as they play a vital role in the design and operational management of PV systems. Accurate parameter identification is indispensable for analysing, assessing, and enhancing the performance of solar energy systems [11–13].

PV cell models are categorized into three main types; single diode, double diode, and three diode models [14]. The single-diode model (SDM), which is known for its simplicity, consists of five unknown parameters, while the double-diode model (DDM) exceeds the SDM in terms of accuracy and includes seven unknown parameters [15]. The most accurate model among them is the three-diode model (TDM), which incorporates nine unknown parameters and is designed to account for factors such as leakage current coefficients and grain boundaries [16]. However, accurately determining the parameters within these PV cell models poses challenges, primarily due to the transcendental nature of the modelling equations and the nonlinear I–V curves [17]. To tackle these challenges and overcome the limitations of analytical and numerical methods, meta-heuristic optimization algorithms have gained significance in the field of PV cell parameter identification [18–20].

The integration of metacognitive algorithms into sustainable energy systems marks a transformative advancement in achieving efficiency and environmental sustainability [21–23]. These algorithms, characterized by their self-reflective and adaptive capabilities, enhance the performance of complex energy systems by learning from historical data and optimizing future operations. This is particularly significant in multi-generation systems that utilize renewable resources such as solar, geothermal, and biomass to produce power, heating, cooling, and freshwater [24–26]. By employing advanced optimization techniques like artificial neural networks and multi-objective optimization, these systems can significantly reduce their environmental impact while maximizing output. The synergy between metacognitive algorithms and sustainable energy technologies fosters innovation and ensures that these systems remain resilient and adaptable amidst evolving environmental challenges [27–29]. This harmonious blend of technology and sustainability not only accelerates the transition to renewable energy but also paves the way for a smarter, greener future. The ability of metacognitive algorithms to continuously improve and adapt makes them indispensable in the quest for sustainable energy solutions, highlighting their crucial role in the development of efficient, resilient, and environmentally friendly energy systems [30]. This integration represents a significant step towards a future where intelligent systems and sustainable practices coexist, driving progress and fostering a more sustainable world.

Meta-heuristic optimization algorithms are inspired by evolutionary concepts, biological behaviours, and physical phenomena to achieve highly efficient convergence, robustness against initial estimates, and a holistic approach to solving optimization problems. Notably, some of these algorithms include the genetic algorithm (GA) [31], transient search optimization [32], northern goshawk optimization algorithm (NGO) [11], particle swarm optimization (PSO) [11], and artificial bee colony (ABC) [33]. These intelligent algorithms typically employ a particle-based methodology, treating model parameters as particles within the search space. Through iterative processes, they evaluate the objective function and update the particles accordingly, until a predetermined termination condition is satisfied. By combining systematic exploration of the search space and interaction between particles, this approach enables the discovery of optimal solutions on a global scale while avoiding local optima.

These algorithms present limitations, such as the potential for being trapped in local optima, longer convergence times due to their iterative nature, and the difficulty of premature convergence, especially in heuristic algorithms. As a result, there is an ongoing effort to develop a precise and appropriate heuristic algorithm for the identification of PV model parameters, which remains a prominent and actively researched area [34]. Within this context, numerous researchers have endeavoured to overcome these limitations by enhancing and customizing intelligent techniques for determining PV model parameters [10, 35].

Over the past few years, researchers have utilized various meta-heuristic optimization methods to address the problems. Some of these methods include the crow whale optimization algorithm(CWOA) [36], genetic algorithm incorporating non-uniform mutation (GAMNU) [31], enhanced JAYA optimization algorithm(EJAYA) [37], improved brain storming optimization algorithm (IBSO) [38], modified SALP swarm optimization (MSSA) [15], innovative optimization algorithm (INFO) [39], northern goshawk optimization (NGO) [11], improved Lozi map based chaotic optimization algorithm (ILCOA) [35]. The main findings from these recent studies are summarized in Table 1.

In spite of their numerous benefits, meta-heuristic methods do come with certain limitations [41]. The operation of all meta-heuristic algorithms can be categorized into two distinct phases, exploration and exploitation. Certain algorithms exhibit a greater emphasis on the exploitation phase, while neglecting the exploration phase. For instance, the PSO and whale optimization algorithm (WOA) encounter a limitation where they become trapped in local minima, thus impeding their capability to accurately search the entire search space [42, 43]. Conversely, other algorithms prioritize the exploration phase, effectively locating the global minimum within

TABLE 1 An overview of the optimization algorithms employed in recent years.

Reference	Proposed algorithm	Model	Fitness function	Primary results
Pourmousa et al. [35]	ILCOA	SDM DDM PVM	RMSE	Impressive local and global search capabilities
Yan et al. [38]	IBSO	SDM DDM	RMSE	IBSO has the potential to deliver highly favourable results
Saadaoui et al. [31]	GAMNU	SDM DDM	RMSE	High-level precision and dependability in competitive performance
Naeijian et al. [40]	WHHO	SDM DDM	RMSE	Robust and rapid strong convergence
Yang and Gong [37]	EJAYA	SDM DDM SMM	RMSE	Enhanced rate of convergence
Yaghoubi et al. [15]	MSSA	SDM DDM PVM	RMSE	MSSA surpasses its rivals and has the potential to generate superior optimal solutions
El-Dabah et al. [39]	INFO	TDM	Combination of the absolute value of the current error	The advantage of INFO in terms of both convergence time and accuracy compared to other optimization techniques

the search space. However, they fail to attain value of the global minimum, as exemplified by the GA and DE algorithms [44, 45]. Necessitating the amalgamation of both exploration and exploitation phases in a harmonious manner, algorithms that present optimal performance are currently being proposed by researchers. Consequently, algorithms that comprise a combination of two distinct algorithms have come to the forefront, such as: PSO-GA, the differential evolution with biogeography-based optimization (DE/BBO) [46, 47]. Another group of researchers improve the performance of the algorithms by adding a part to the classical algorithms. Some of these algorithms are used in this article to compare with the proposed method, like flexible particle swarm optimization (FPSO) [10], whippy Harris Hawks optimization (WHHO) [40], springy whale optimization algorithm (SWOA) [48], repairable grey wolf optimization algorithm (RGWO) [49] and so on [50–54].

In this paper, we introduce a novel method that can be seamlessly integrated into any metacognitive algorithm to enhance its performance, particularly in avoiding entrapment in local minima. The proposed algorithm is structured around two main phases: elimination and search space control. During the elimination phase, once a specific condition is met, the algorithm removes a percentage of the population with the poorest performance and replaces it with a new, randomly distributed population that has no prior experience in the search space. This approach helps the algorithm escape local minima by exploring new areas of the search space. In the search space control phase, the goal is to thoroughly search the entire space for the global minimum. Initially, the population is confined to a small region of the search space, which gradually expands until the entire space is covered. This method can be easily implemented on any metacognitive algorithm. Given the grasshopper optimization algorithm's (GOA) challenges in overcoming local minima [55], we implemented our method on GOA, resulting in the bio dynamics grasshopper optimization algorithm (BDGOA).

One of the advantages of this method is its simplicity, as it does not necessitate intricate calculations to reduce the algorithm's speed. The algorithm exhibits exceptional convergence speed and remarkable efficiency in locating the global optimal point while avoiding local minima. The performance evaluation of the BDGOA algorithm involved its application in identifying and extracting the unknown parameters of five solar modules: R.T.C France [56], PWP201 [57], SM55 [58], KC200GT [58], and SW255 [59]. Initially, the unknown parameters of various RTC France and PWP201 models were identified, followed by verification of the extracted parameters' validity through comparison with experimental models under diverse temperature and radiation conditions. Furthermore, the impact of radiation and temperature on the parameters of the mentioned modules is elucidated and analysed. Subsequently, the effects of BDGOA algorithm parameters on convergence speed and escaping local minima are discussed. Finally, the significance of accurately identifying solar cell parameters in the industry and the resulting cost savings is highlighted.

The article further details the implementation, which can be summarized as follows:

- Implementing the elimination phase: removing the worst locusts (potential solutions) and replacing them with new random grasshoppers and spreading them in a space away from the local minimum.
- Controlling the search space: considering a small part of the state space and rarely making it larger.

The subsequent sections of the paper are structured as follows. Section 2 introduces the model of the photovoltaic (PV) cell and module, along with the corresponding relationships.

Section 3 presents and formulates the proposed algorithm. Section 4 provides simulations and analyses the obtained results. Ultimately, Section 5 articulates the concluding remarks.

2 | MATHEMATICAL MODELING AND PROBLEM FORMULATION

This section, some of the most popular mathematics models of solar cell (SD, DD, and TD) and also PV module models are introduced which are used a lot in practice.

2.1 | Photovoltaic cell model

2.1.1 | Single-diode model

As can be seen from Figure 1, the structure of this model consists of a diode, a series resistance (R_s), a shunt resistance (R_{sh}) and a current source (I_{ph}) [10]. Although the structure of this model is very simple, it is widely used in practice due to its proper accuracy of solar cell behaviour. The output current (I_t) can be calculated as follows [40]:

$$I_t = I_{ph} - I_{sh} - I_d \tag{1}$$

where I_{sh} and I_d denote shunt resistance current and the diode current, respectively. Their equations are as follow:

$$I_{sh} = \frac{V_t + I_t.R_s}{R_{sh}} \tag{2}$$

$$I_d = I_{sd}\left[\exp\left(\frac{q\,(V_t + R_s.I_t)}{n.k.T}\right) - 1\right] \tag{3}$$

In which, V_t is terminal voltage, I_{sd} is the diode reverse saturation current, n is the diode ideality factor, $q = 1.602 \times 10^{-19}$ is the magnitude of charge on an electron, $k = 1.381 \times 10^{-23}$ (J/K) is the Boltzmann constant and T is the cell temperature (K). Then, I_t can be rewritten as follows [35]:

$$I_t = I_{ph} - \frac{V_t + I_t.R_s}{R_{sh}} - I_{sd}\left[\exp\left(\frac{q\,(V_t + R_s.I_t)}{n.k.T}\right) - 1\right] \tag{4}$$

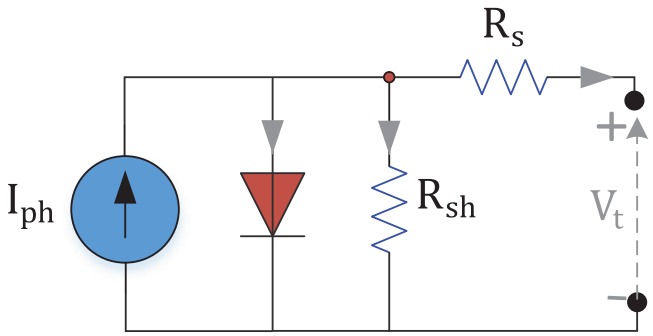

FIGURE 1 Single diode model's equivalent circuit.

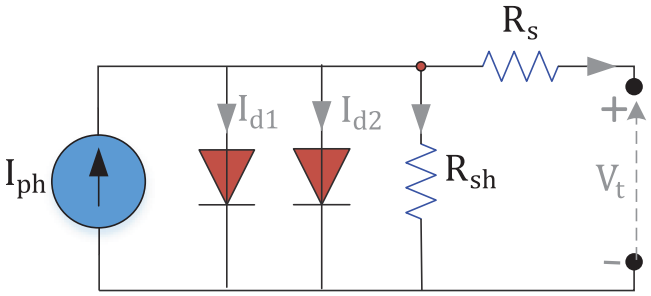

FIGURE 2 Double diode model's equivalent circuit.

From Equation (4), it is clear that the five unknown parameters to be identified are:

$$\theta = \left[I_{ph}, R_s, R_{sh}, I_{sd}, n\right] \tag{5}$$

2.1.2 | Double-diode model

Although SDM is considered an accurate model in engineering, researchers needed a more accurate model for specific applications. For this reason, they presented the double-diode model. In this model, as can be seen from Figure 2, there is one more diode compared to SDM, which has led to the creation of 7 unknown parameters. The first diode is set as a rectifier and the second diode models the charge recombination current. The output current is obtained as follows:

$$I_t = I_{ph} - I_{sh} - I_{d_1} - I_{d_2} \tag{6}$$

As before, Equation (6) can be rewritten using Equations (2) and (3) as follows:

$$I_t = I_{ph} - \frac{V_t + I_t.R_s}{R_{sh}} - I_{sd_1}\left[\exp\left(\frac{q\,(V_t + R_s.I_t)}{n_1.k.T}\right) - 1\right] - I_{sd_2}\left[\exp\left(\frac{q\,(V_t + R_s.I_t)}{n_2.k.T}\right) - 1\right] \tag{7}$$

Where $(I_{ph}, R_s, R_{sh}, I_{sd_1}, I_{sd_2}, n_1, n_2)$ are unknown parameters.

2.1.3 | Triple-diode model

The three-diode model, which is more accurate than the previous two models, is used less in practice. This model has 9 unknown parameters $(I_{ph}, R_s, R_{sh}, I_{sd_1}, I_{sd_2}, I_{sd_3}, n_1, n_2, n_3)$ that can challenge the proposed algorithm. According to Figure 3, the output current is calculated as follows [48]:

$$I_t = I_{ph} - I_{sh} - I_{d_1} - I_{d_2} - I_{d_3} \tag{8}$$

Thus, the output current can be rewritten as follows:

$$I_t = I_{ph} - \frac{V_t + I_t.R_s}{R_{sh}} - I_{sd_1}\left[\exp\left(\frac{q\,(V_t + R_s.I_t)}{n_1.k.T}\right) - 1\right]$$

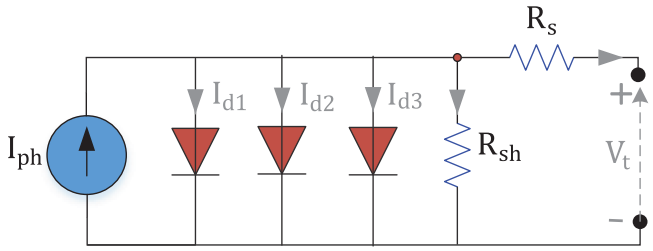

FIGURE 3 Triple diode model's equivalent circuit.

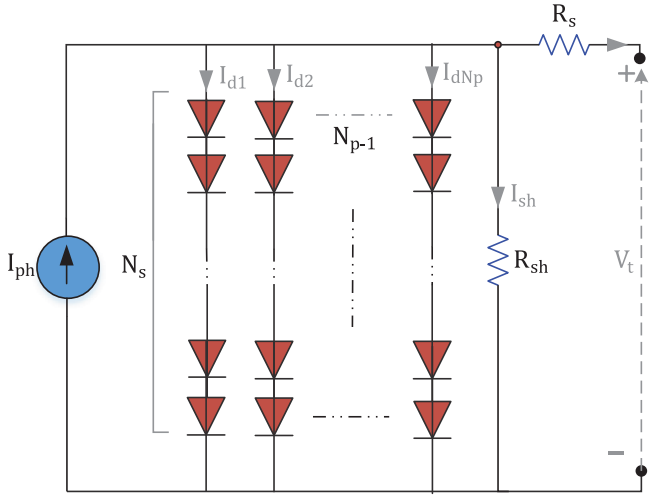

FIGURE 4 PV model's equivalent circuit.

$$- I_{sd_2}\left[\exp\left(\frac{q\,(V_t + R_s.I_t)}{n_2.k.T}\right) - 1\right]$$
$$- I_{sd_3}\left[\exp\left(\frac{q\,(V_t + R_s.I_t)}{n_3.k.T}\right) - 1\right] \quad (9)$$

2.2 | PV module model

A PV module is made of a number of solar cells which are connected to each other in series and/or parallel to form the single-diode PV module illustrated in Figure 4. The output current of a single-diode (SDM) PV module can be calculated using Equation (10).

$$I_t = N_p.I_{ph} - \frac{N_p.V_t/N_s + I_t.R_s}{R_{sh}} - N_p.I_{sd}\left[\exp\left(\frac{q\,(V_t/N_s + R_s.I_t/N_p)}{n.k.T}\right) - 1\right] \quad (10)$$

where N_p and N_s are the number of solar cells in parallel and series, respectively. As mentioned in the Section 1, the behaviour of the solar cell system is dependent on the amount of temperature and irradiance, and if we want to check the performance of the system in different conditions of temperature and irradiance, it is necessary to rewrite the above equation using the following equations:

$$I_{ph} = \left(I_{ph\_STC} + K_i\Delta T\right)\frac{G}{G_{STC}} \quad (11)$$

Where, I_{ph_STC} (in Ampere) is the light generated current at STC, $\Delta T = T - T_{STC}$ (in Kelvin, $T_{STC} = 25\ ^\circ C$), G is the surface irradiance of the cell and G_{STC} (1000 w/m^2) is the irradiance at STC. The constant K_i is the short-circuit current coefficient, normally provided by the manufacturer. An equation to describe the saturation current which considers the temperature variation is given by [10]:

$$I_{sd} = \frac{\left(I_{SC\_STC} + K_i\Delta T\right)}{\exp\left[\frac{q\left(V_{OC\_STC} + K_v\Delta T\right)}{n.k.T}\right] - 1} \quad (12)$$

The constant K_v is the open circuit voltage coefficient. This value is available from the datasheet.

2.3 | Objective function

Figure 5 illustrates an overview of the identification of solar module parameters. As it is clear, with the solar irradiance, the output voltage and current are received to be given as necessary input to the PV cell model. After that, the proposed algorithm tries to find the unknown parameters of the system so that finally the estimated current (I_{est}) and the output current become the same. For this purpose, it needs a cost function which is as follows:

$$F(\theta) = \mathrm{RMSE}(\theta) = \sqrt{\frac{1}{N_E}\sum_{i=1}^{N_E} f_M(V_t, I_t, \theta)^2} \quad (13)$$

where N_E represents the number of measured data and M is used for determining the SDM, DDM, TDM, and the PV panel. The objective function for them is displayed in Equations (13)–(16), respectively:

$$f_{SDM}(V_t, I_t, \theta) = \theta_1 - \frac{V_t + I_t.\theta_2}{\theta_3} - \theta_4\left[\exp\left(\frac{q\,(V_t + \theta_2.I_t)}{\theta_5.k.T}\right) - 1\right] - I_t \quad (14)$$

$$f_{DDM}(V_t, I_t, \theta) = \theta_1 - \frac{V_t + I_t.\theta_2}{\theta_3} - \theta_4\left[\exp\left(\frac{q\,(V_t + \theta_2.I_t)}{\theta_6.k.T}\right) - 1\right] - \theta_5\left[\exp\left(\frac{q\,(V_t + \theta_2.I_t)}{\theta_7.k.T}\right) - 1\right] - I_t \quad (15)$$

$$f_{DDM}(V_t, I_t, \theta) = \theta_1 - \frac{V_t + I_t.\theta_2}{\theta_3} - \theta_4\left[\exp\left(\frac{q\,(V_t + \theta_2.I_t)}{\theta_7.k.T}\right) - 1\right] - \theta_5\left[\exp\left(\frac{q\,(V_t + \theta_2.I_t)}{\theta_8.k.T}\right) - 1\right] - \theta_6\left[\exp\left(\frac{q\,(V_t + \theta_2.I_t)}{\theta_9.k.T}\right) - 1\right] - I_t \quad (16)$$

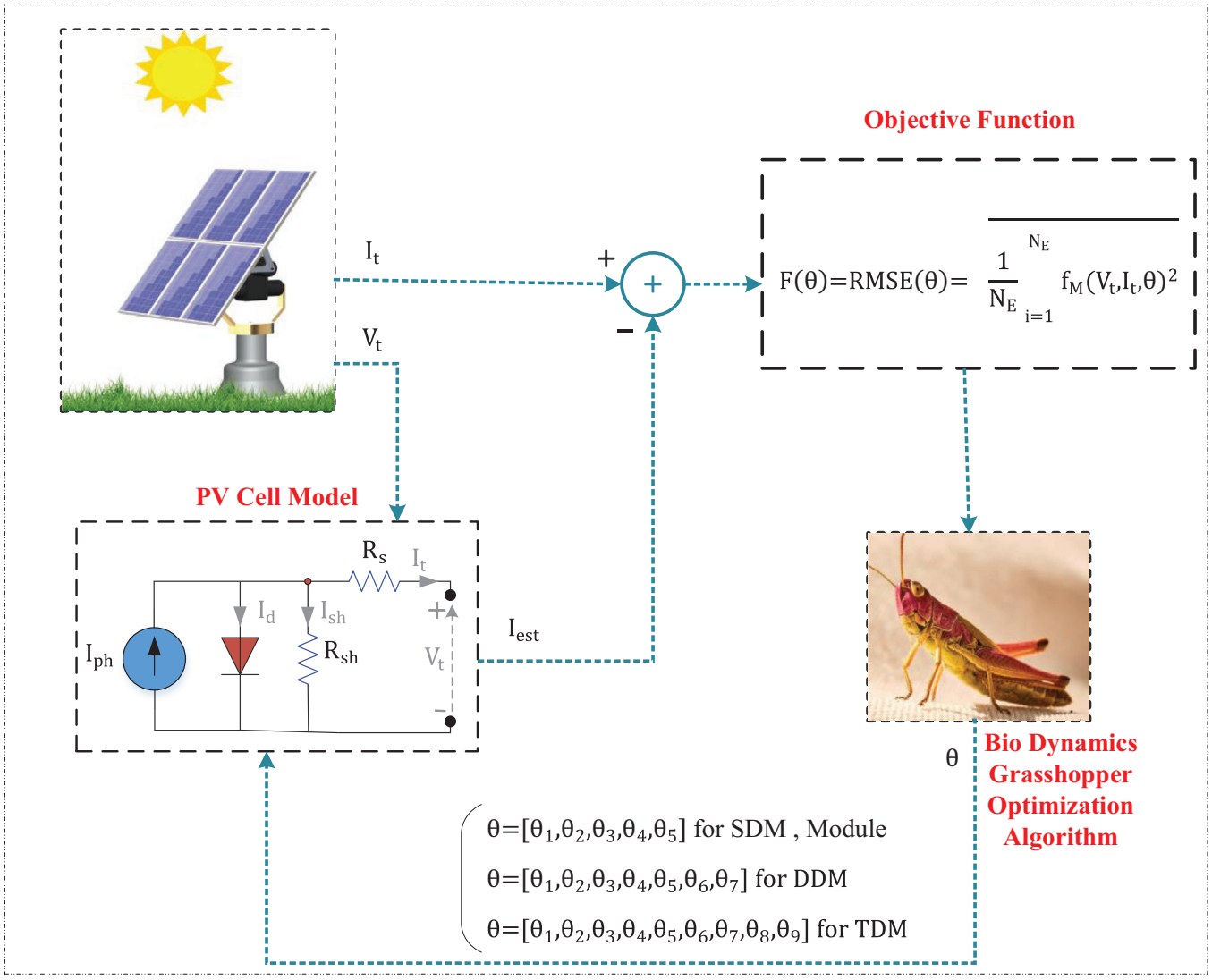

FIGURE 5 Overview for parameters estimation of PV cell models using BDGOA.

$$f_{\text{panel}}(V_t, I_t, \theta) = \theta_1 - \frac{V_t + I_t.\theta_2.N}{\theta_3.N} - \theta_4\left[\exp\left(\frac{q(V_t + \theta_2.I_t.N)}{\theta_5.k.T.N}\right) - 1\right] - I_t \quad (17)$$

The unknown parameters vector is in the form of $\theta = [\theta_1, \theta_2, \theta_3, \theta_4, \theta_5]$ for the SDM and the PV panel, is in the form of $\theta = [\theta_1, \theta_2, \theta_3, \theta_4, \theta_5, \theta_6, \theta_7]$ for the DDM and is in the form of $\theta = [\theta_1, \theta_2, \theta_3, \theta_4, \theta_5, \theta_6, \theta_7, \theta_8, \theta_9]$ for the TDM.

3 | GRASSHOPPER ALGORITHM

The GOA is a meta-heuristic optimization method that has been placed in the category of population-based algorithms due to its inspiration from the group behaviour of grasshopper. Grasshopper to search for food (the best solution), first with long-range jumps, spread almost all over the agricultural land (search space) (exploration phase) and then move locally with small steps to achieve the best food source (exploitation phase). The mathematical model of the position of the grasshoppers (the solution to the optimization problem) can be modelled according to three factors affecting the movement of the grasshoppers, which include the social interaction (S_i), the gravity force on the grasshopper (G_i), and wind advection (A_i) [45].

$$X_i = S_i + G_i + A_i \quad (18)$$

And

$$S_i = \sum_{\substack{j=1 \\ j \neq i}}^{N} s\left(d_{ij}\right)\hat{d}_{ij} \quad (19)$$

Where $d_{ij} = |x_j - x_i|$ is the distance between ith and jth grasshopper, $\hat{d}_{ij} = \frac{x_j - x_i}{d_{ij}}$ is an unit vector from ith to jth grasshopper and $s(r) = fe^{\frac{-r}{l}} - e^{-r}$ is the social forces strength

which can be adjusted by two parameters (l is the attractive length scale and f is the attraction intensity).

In Equation (18), G_i and A_i are given in Equation (20) [55].

$$G_i = -g\hat{e}_g, A_i = u\,\hat{e}_w \tag{20}$$

In which, g is constant of gravity, u is constant drift, $\hat{e}_g$ and $\hat{e}_w$ indicate unity vector towards earth center and unity vector in the wind direction, respectively. So, Equation (18) is rewritten by substituting Equations (19) and (20) as follows:

$$X_i = \sum_{\substack{j=1 \\ j\neq i}}^{N} s\left(\left|x_j - x_i\right|\right)\frac{x_j - x_i}{d_{ij}} + -g\hat{e}_g + u\,\hat{e}_w \tag{21}$$

where N is the number of grasshoppers. Equation (21) is inspired by the behaviour of grasshoppers, but during several experiments, it was found that it cannot perform well in solving optimization problems. For this reason, some special parameters were added to the mathematical model, which resulted in a good balance between exploration and exploitation:

$$X_i = \mathrm{c}\left(\sum_{\substack{j=1 \\ j\neq i}}^{N} c\frac{\mathrm{ub}_d - \mathrm{lb}_d}{2} s\left(\left|x_j^{\mathrm{d}} - x_i^{\mathrm{d}}\right|\right)\frac{x_j - x_i}{d_{ij}}\right) + T_d \tag{22}$$

In Equation (22), ub_d and lb_d are the upper and lower bounds in the dth dimension of $s(r)$, respectively. T_d indicates value of the dth dimension in the target (best solution) and c is a decreasing coefficient to shrink the comfort zone defined as the zone in the search space that the GOA algorithm can use it to establish a suitable balance between exploration and exploitation. As the number of iterations increases, the exploration part decreases and the exploitation part increases according to the following equation:

$$\mathrm{c} = c_{\max} - it\frac{c_{\max} - c_{\min}}{L} \tag{23}$$

In which, it is the current iteration, $c_{\max}$ and $c_{\min}$ are the maximum and the minimum value, respectively and L indicates the maximum number of iterations.

3.1 | Swift grasshopper optimization algorithm

The correctness of the information mentioned in the relevant articles about the disadvantages of the algorithm is confirmed by the review and tests that have been carried out on the grasshopper algorithm in order to be used in optimization problems. Some of the most serious drawbacks are the algorithm's slow convergence speed, poor ability to find a large number of unknown system parameters, and getting stuck in local minima. The very low speed of convergence of this algorithm caused a new version of the algorithm to be presented by Mirjalili et al., whose MATLAB code is provided on the website of the Grasshopper algorithm. But its convergence speed is still much lower than many algorithms.

However, the GOA algorithm tends to get stuck in local minima that one of the main reasons is the way of updating the c parameter. As can be seen from Equation (23), the parameter c becomes smaller and approaches the $c_{\min}$ value by increasing the number of iterations, and thus exerts all its effort on the exploitation phase regardless of the exploitation phase. To solve these disadvantages, we have proposed the bio dynamics grasshopper optimization algorithm (BDGOA).

In the BDGOA, some simple but very effective ideas have been used. First idea is to eliminate a number of underperforming grasshoppers (the worst solution) during iteration and randomly distribute new grasshoppers in new regions of the search space. In this way, a very good balance is created between exploitation and exploration. This process includes providing additional parameters (ep, et, Th, w) of the grasshopper algorithm. Figure 6 shows the flowchart of the proposed algorithm, the changes applied to the GOA algorithm are shown in blue.

The new design parameters allow for a suitable balance between exploration and exploitation. During this method, the total population of grasshoppers remains constant and after et of the total iteration, the value of the objective function is calculated for all grasshoppers. Then ep number of the least active grasshoppers (worst answers) are removed and replaced with new Grasshoppers in random regions of the search space. For further explanation, the BDGOA is used to find the optimal point of the Rastrigin function (Figure 7). The search space is [−5.12, 5.12] and other parameters were selected as follows: ($L = 140, N = 50, ep = 15, et = 25$).

As can be clearly seen from Figure 6, the proposed algorithm does not enter the elimination phase until the constraint condition is confirmed. So, the algorithm continues its previous process until the 24th iteration and does not enter the constraint condition. But in the 25th iteration, it enters the elimination phase and removes underperforming grasshoppers and distributes new locusts randomly in the search space. Note that the best grasshoppers are not removed and remain, some of which are shown in red dashed circle in Figure 7. Since the total number of repetitions is 140, this algorithm enters the elimination loop 7 times in total. White dots represent locusts.

The second idea is to control the search space so that the algorithm searches the entire search space to find the best answer (global minimum) with much greater precision.

This operation, which is performed using, Th and w parameters, initially, locusts search in a limited search space. After a certain criterion is met (for example, a percentage of the maximum iteration), the search space grows larger with a growth rate w. This process continues until the search space is equal to the entire search space. Another advantage of this method is that it is not necessary to select a large number of locusts like the GOA algorithm, but the best solution can be reached with a smaller number of locusts. As a result, the execution time of the algorithm is less than the classic GOA algorithm, which leads to faster convergence to the global solution.

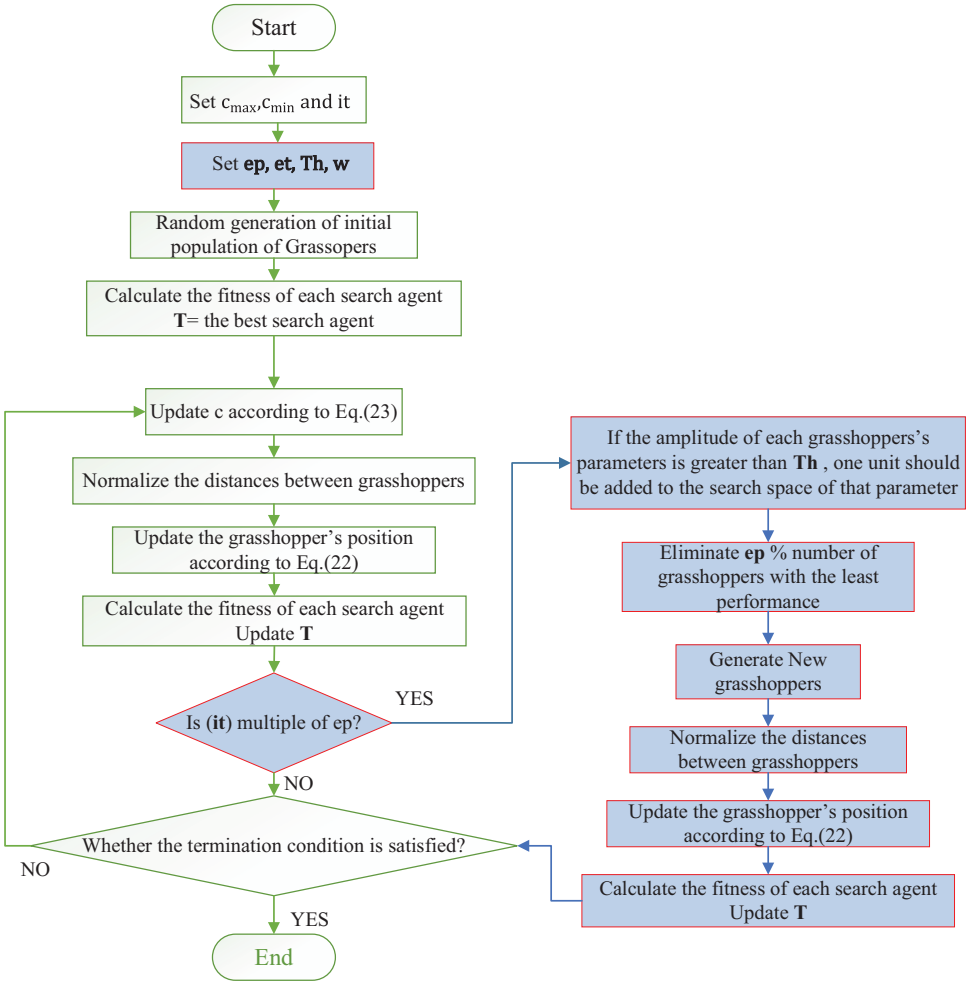

FIGURE 6 Flowchart of BDGOA algorithm.

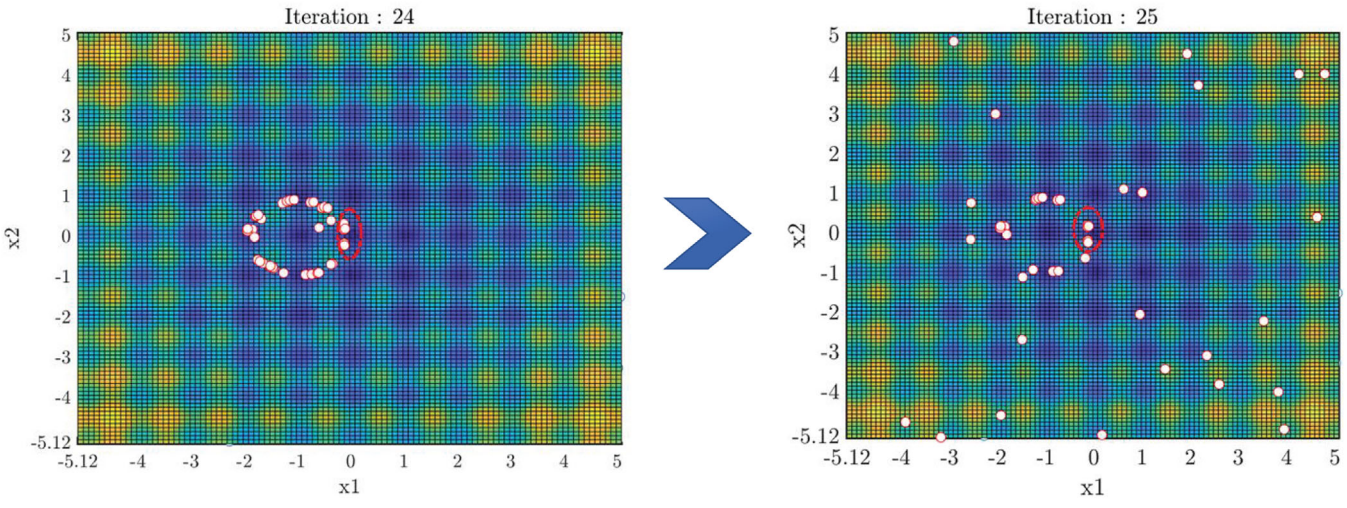

FIGURE 7 Found the minimum value of the Rastrigen function by BDGOA, a) before eliminate phase, b) after eliminate phase.

TABLE 2 Experimental data of the investigated modules under STC.

Parameters	SM55	KC200GT	SW255
Maximum power ($P_{max}(W)$)	55	200	255
Voltage at P_{max} ($V_{ppm}(V)$)	17.4	26.3	31.4
Current at P_{max} ($I_{ppm}(A)$)	3.15	7.61	8.15
Open circuit voltage ($V_{oc}(V)$)	21.7	32.9	37.8
Short circuit Current ($I_{sc}(A)$)	3.45	8.21	8.66
K_V (mV/°C)	−76	−123	−30
K_I (mA/°C)	1.40	3.18	4
Number of cells	36	54	60

4 | SIMULATIONS

In this section, the performance evaluation of the BDGOA algorithm is conducted by identifying the unknown parameters of several widely-used solar systems in the industry. The identified systems include R.T.C France, with a diameter of 57 mm, Photowatt-PWP201, consisting of 36 polycrystalline-type solar cells, SM55 (monocrystalline), KC200GT (multi-crystalline), and SW255 (polycrystalline). These systems are tested under varying irradiance and temperature conditions, with their specifications provided in Table 2.

In the initial phase, the unknown parameters of RTC France and PWP201 systems are identified in all models: single diode, two diodes, and three diodes. Subsequently, the impact of irradiance and temperature on the SM55, KC200GT, and SW255 modules is investigated in the following part. The search space of the unknown parameters can be referred to in Table 3.

Furthermore, in addition to the BDGOA algorithm, twelve meta-heuristic algorithms are compared. The selected algorithms include the latest ones such as FPSO, WHHO, and SWOA, along with well-known algorithms like GA and PSO to ensure a comprehensive and unbiased comparison. For all systems, a fixed number of iterations, namely 5000, is employed and the parameters of each algorithm are chosen and adjusted based on pertinent references, aiming to maximize their performance. The simulations are administered using the MATLAB 2020b environment.

4.1 | Parameters identification of R.T.C France solar cell

One of the most commonly utilized solar modules is R.T.C France, which is extensively referenced in scholarly literature. Table 4 presents a comprehensive dataset comprising measured voltage and current values of the RTC module, utilized for determining unknown parameters. The subsequent columns of this table display the estimated current by the proposed algorithm in three models: single diode, two diodes, and three diodes. The respective relative error, formulated as follows [10]:

$$R_{err} = \frac{I_t - I_{est}}{I_{est}} \quad (2)$$

From an examination of Table 4, it is evident that the relative error is negligibly low, indicating similarity between the estimated and measured current values. Furthermore, upon careful scrutiny of this table, it can be observed that the error value in the three-diode model is lower compared to the single-diode model, thus signifying the greater accuracy of the three-diode model in comparison.

Table 5 demonstrates the unidentified parameter values identified by the BDGOA algorithm and 12 alternative algorithms. It can be inferred from the table that half of the utilized algorithms, similar to the BDGOA algorithm, were capable of achieving the lowest RMSE (root mean square error) value. Accordingly, for further investigation, the convergence speed of these algorithms is compared with that of the proposed algorithm (Figure 8). It is evident from this figure that the BDGOA algorithm exhibits the fastest convergence speed, whereas the GOA algorithm showcases the slowest convergence speed, initially encountering a local minimum.

Tables 6 and 7 showcase the values of the unidentified parameters established for the two-diode and three-diode models, respectively. In these models, due to the increased number of unknown parameters compared to the single diode model, the algorithms face greater challenges. However, the BDGOA algorithm managed to achieve the lowest RMSE value, followed by the WHHO and SWOA algorithms. Convergence speeds of the algorithms for the two-diode and three-diode models are presented in Figures 9 and 10, respectively. It is apparent from these figures that the proposed algorithm possesses the highest

TABLE 3 Parameters ranges of PV modules.

	RTC France PV		PWP201		PV module	
Parameter	Lower bound	Upper bound	Lower bound	Upper bound	Lower bound	Upper bound
I_{ph} (A)	0	1	0	2	0	$2I_{SC}$
I_{sd}, I_{sd2}, I_{sd3} (μA)	0	1	0	50	0	100
R_s (Ω)	0	0.5	0	2	0	2
R_{sh} (Ω)	0	100	0	1000	0	5000
n_1, n_2	1	2	1	50	1	4
n_3	2	5	1	50		

TABLE 4 Relative error for each measurement.

			SDM		DDM		TDM	
DATA	V_L (V)	I_L (A)	I_{te} (A)	R_{err}	I_{te} (A)	R_{err}	I_{te} (A)	R_{err}
1	−0.2057	0.7640	0.76408	−0.00011	0.76398	0.00002	0.76397	0.00003
2	−0.1291	0.7620	0.76266	−0.00086	0.76260	−0.00079	0.76260	−0.00078
3	−0.0588	0.7605	0.76135	−0.00112	0.76133	−0.00109	0.76133	−0.00109
4	0.0057	0.7605	0.76015	0.00045	0.76017	0.00042	0.76017	0.00042
5	0.0646	0.7600	0.75905	0.00124	0.75910	0.00117	0.75911	0.00116
6	0.1185	0.7590	0.75804	0.00126	0.75812	0.00115	0.75812	0.00114
7	0.1678	0.7570	0.75709	−0.00012	0.75718	−0.00024	0.75719	−0.00025
8	0.2132	0.7570	0.75614	0.00113	0.75624	0.00099	0.75624	0.00099
9	0.2545	0.7555	0.75508	0.00054	0.75517	0.00042	0.75517	0.00042
10	0.2924	0.7540	0.75366	0.00044	0.75372	0.00036	0.75371	0.00038
11	0.3269	0.7505	0.75138	−0.00118	0.75139	−0.00119	0.75136	−0.00115
12	0.3585	0.7465	0.74734	−0.00113	0.74729	−0.00106	0.74723	−0.00098
13	0.3873	0.7385	0.74009	−0.00215	0.7399	−0.00201	0.73987	−0.00185
14	0.4137	0.7280	0.72739	0.00082	0.72726	0.00101	0.72703	0.00132
15	0.4373	0.7065	0.70695	−0.00064	0.70683	−0.00047	0.70641	0.00012
16	0.4590	0.6755	0.67529	0.00030	0.67523	0.00039	0.67450	0.00147
17	0.4784	0.6320	0.63088	0.00176	0.63088	0.00176	0.62975	0.00357
18	0.4960	0.5730	0.57208	0.00160	0.57214	0.00150	0.57047	0.00442
19	0.5119	0.4990	0.49949	−0.00098	0.49957	−0.00114	0.49730	0.00340
20	0.5265	0.4130	0.41349	−0.00119	0.41355	−0.00134	0.41063	0.00575
21	0.5398	0.3165	0.31721	−0.00226	0.31724	−0.00233	0.31366	0.00902
22	0.5521	0.2120	0.21210	−0.00048	0.21208	−0.00038	0.20786	0.01986
23	0.5633	0.1035	0.10272	0.00758	0.10267	0.00806	0.097869	0.05753
24	0.5736	−0.0100	−0.00924	0.08121	−0.00929	0.07560	−0.01463	−0.31693
25	0.5833	−0.1230	−0.12438	−0.01110	−0.12439	−0.01117	−0.13023	−0.05552
26	0.5900	−0.2100	−0.20919	0.00385	−0.20914	0.00407	−0.21532	−0.02471

TABLE 5 Detailed results for SDM of RTC France.

Algorithms	I_{ph} (A)	I_{sd} (μA)	n	R_s (Ω)	R_{sh} (Ω)	RMSE
BDGOA	**0.760775**	**0.323019**	**1.48110**	**0.036377**	**53.718660**	$\mathbf{9.860218 \times 10^{-4}}$
GOA	0.770029	0.258316	1.458500	0.048315	62.477562	2.0623×10^{-2}
LGOA	0.760891	0.338992	1.4861	0.0361998	53.2146	1.0944×10^{-3}
FPSO	0.7607	0.3230	1.4811	0.03637	53.7185	9.8602×10^{-4}
WHHO	0.76077551	0.3230231	1.48110808	0.03637710	53.71867407	9.8602×10^{-4}
SWOA	0.76077551	0.32302318	1.48110897	0.03637706	53.71886754	9.8602×10^{-4}
RGWO	0.76077553	0.323020823	1.48118359	0.03637709	53.7185261	9.8602×10^{-4}
ILCOA	0.760775	0.323021	1.481108	0.036377	53.718679	9.86021×10^{-4}
EHHO [30]	0.760775	0.323	1.481238	0.036375	53.74282	9.8602×10^{-4}
WOA	0.76075413	0.3243611	1.4815199	0.03636524	54.10454052	9.8615×10^{-4}
LCOA [25]	0.760752	0.323278	1.481187	0.036374	53.902365	9.86094×10^{-4}
PSO	0.7607	0.400	1.5033	0.0354	59.012	1.38×10^{-3}
GA	0.7619	0.8087	1.5751	0.0299	42.3729	1.8704×10^{-2}

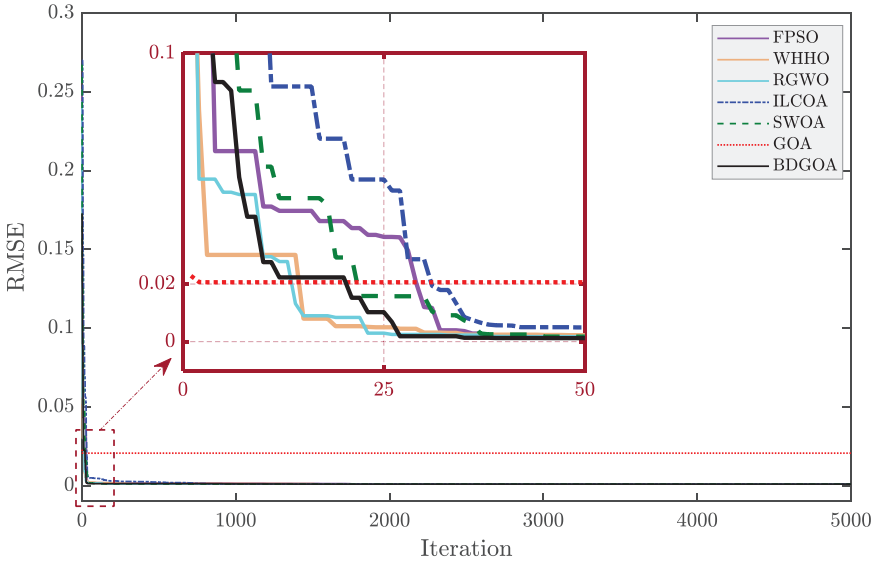

FIGURE 8 RMSE evolution of the algorithms for the SDM.

TABLE 6 Detailed results for DDM of RTC France.

Algorithms	I_{ph} (A)	I_{sd1} (μA)	I_{sd2} (μA)	n_1	n_2	R_s (Ω)	R_{sh} (Ω)	RMSE
BDGOA	**0.76078**	**0.22625**	**0.74722**	**1.45104**	**2**	**0.03673**	**55.48023**	$\mathbf{9.82473 \times 10^{-4}}$
GOA [7]	0.76077	0.21	0.21	1.45651	1.551	0.033662	55.2016	5.8864×10^{-2}
LGOA [7]	0.76077	0.21	0.21	1.4497	1.6745	0.03666	55.2016	9.9691×10^{-4}
FPSO	0.76078	0.22731	0.72786	1.45160	1.99969	0.036737	55.3923	9.8253×10^{-4}
WHHO	0.76078	0.22857	0.72718	1.45189	2	0.03672	55.42643	9.82487×10^{-4}
SWOA	0.76078	0.70757	0.23082	2	1.452711	0.036719	55.371095	9.8249×10^{-4}
RGWO	0.76078	0.22718	0.74714	1.45144	0.760781	0.03672	55.54442	9.82511×10^{-4}
ILCOA	0.76078	0.22601	0.74921	1.45101	2.00000	0.036739	55.5320	9.8257×10^{-4}
EHHO	0.76076	0.58618	0.24096	1.968451	1.4569104	0.0365988	55.6394395	9.83606×10^{-4}
WOA	0.76077	0.26185	0.22162	1.4645250	1.82539530	0.0365306	54.3404740	9.8464×10^{-4}
LCOA	0.76077	0.26612	0.38023	1.46205	1.9938	0.3667	54.6314	9.8423×10^{-4}
PSO	0.7623	0.4767	0.0102	1.5172	2	0.0325	43.1034	1.6600×10^{-3}
GA	0.7608	0.0001	0.0001	1.3355	1.481	0.0364	53.7185	3.6040×10^{-1}

TABLE 7 Detailed results for TDM of RTC France.

Algorithms	I_{ph} (A)	I_{sd1} (μA)	I_{sd2} (μA)	I_{sd3} (μA)	n_1	n_2	n_3	R_s (Ω)	R_{sh} (Ω)	RMSE
BDGOA	**0.76078**	**0.44311**	**0.23891**	**0.8**	**2**	**1.45387**	**2.40708**	**0.03672**	**55.65355**	$\mathbf{9.807313 \times 10^{-4}}$
GOA	0.76078	0.15071	0.29995	0.14490	1.99999	1.47352	2.83395	0.03645	54.05813	9.84385×10^{-4}
LGOA	0.760781	0.22842	0.57977	0.5851	1.45129	2	2.38495	0.03176	55.78076	9.81148×10^{-4}
FPSO	0.7607	0.2225	0.7467	0.2353	1.4495	2	2.5851	0.0367	55.7531	9.8203×10^{-4}
WHHO	0.76078	0.23910	0.43972	0.8	1.45393	2	2.40415	0.03672	55.64995	9.80751×10^{-4}
SWOA	0.76078	0.24204	0.36359	1	1.45602	2	2.40819	0.03672	55.69461	9.8033×10^{-4}
RGWO	0.76078	0.49872	0.23049	0.67753	1.99999	1.45090	2.32581	0.03675	55.78999	9.81064×10^{-4}
ILCOA	0.7607	0.2231	0.7390	0.2226	1.4497	2	2.5771	0.0367	55.6554	9.8204×10^{-4}
EHHO	0.76078	0.22854	0.57999	0.5861	1.45029	2	2.39655	0.03676	55.77064	9.81232×10^{-4}
WOA	0.76077	0.2353	0.2213	0.4573	1.4543	1.4978	2	0.03668	55.4448	9.8249×10^{-4}
LCOA	0.76078	0.22844	0.57979	0.5858	1.44929	2	2.39450	0.03471	55.78074	9.81754×10^{-4}
PSO	0.7607	0.2259	0.7491	0.0023	1.4509	2	2.3156	0.0367	55.47571	9.8247×10^{-4}
GA	0.7605	0.3251	0.3608	0	1.4843	1.9975	2.2099	0.0357	58.6086	1.0531×10^{-3}

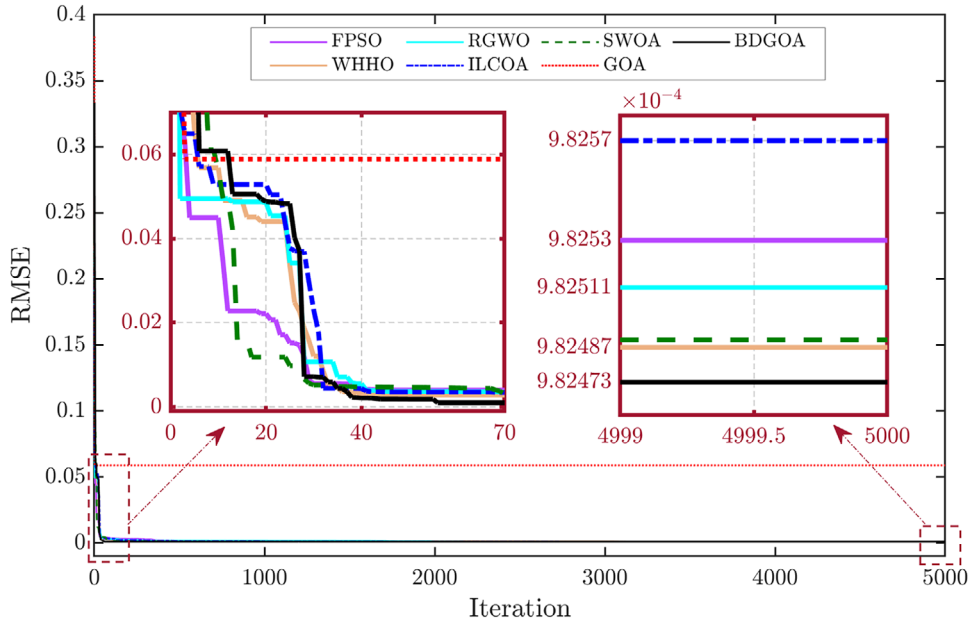

FIGURE 9 RMSE evolution of the algorithms for the DDM.

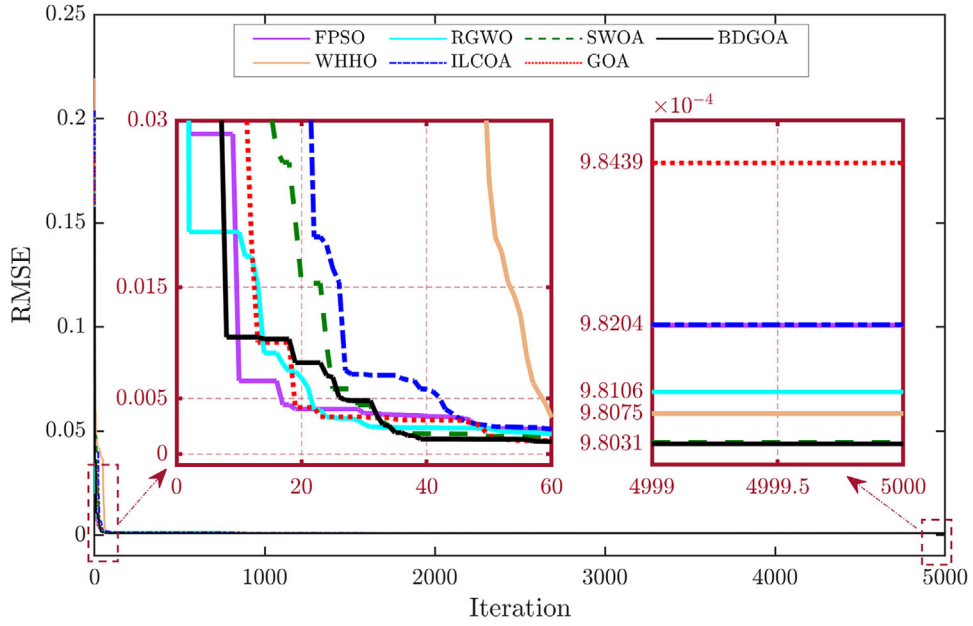

FIGURE 10 RMSE evolution of the algorithms for the TDM.

convergence speed. After assessing the convergence speed of the algorithms, their resistance and stability are evaluated. In this assessment, each algorithm was executed 30 times, and the outcomes are provided in Table 8. Table 8 indicates that the BDGOA algorithm exhibits highly favourable resistance, as it attains the lowest value within 30 iterations in the single diode and two-diode models. Notably, the three-diode model also demonstrates acceptable stability.

4.2 | Parameters identification of photowatt-PWP201 PV module

The PWP201 is a commercial photovoltaic module that consists of 36 polycrystal cells. The measured current and voltage of the PWP201 module are displayed in the second and third columns of Table 9, while the remaining columns represent the current detected by the proposed algorithm in the single-diode,

TABLE 8 Comparison between RMSE values for the SDM, DDM, TDM of RTC France obtained by different algorithms after 30 runs.

Algorithm	BDGOA	GOA	LGOA	FPSO	WHHO	SWOA	RGWO	ILCOA	EHHO	WOA	LCOA	PSO	GA
SDM													
Min	**9.860218×10^{-4}**	2.0623×10^{-2}	1.0944×10^{-3}	9.8602×10^{-4}	9.8602×10^{-4}	9.8602×10^{-4}	9.8602×10^{-4}	9.860218×10^{-4}	9.8602×10^{-4}	9.8615×10^{-4}	9.860945×10^{-4}	1.38×10^{-3}	1.8704×10^{-2}
Mean	**9.860218×10^{-4}**	2.99×10^{-2}	1.8110×10^{-3}	9.8602×10^{-4}	9.8602×10^{-4}	9.8602×10^{-4}	9.8602×10^{-4}	9.8839×10^{-4}	9.8645×10^{-4}	9.8621×10^{-4}	9.9421×10^{-4}	1.4161×10^{-3}	1.9903×10^{-2}
Max	**9.860218×10^{-4}**	4.53×10^{-2}	3.0010×10^{-3}	9.8602×10^{-4}	9.8602×10^{-4}	9.8602×10^{-4}	9.8602×10^{-4}	9.9484×10^{-4}	9.8862×10^{-4}	9.8798×10^{-4}	9.9821×10^{-4}	1.5123×10^{-3}	2.5146×10^{-2}
DDM													
Min	**9.82473×10^{-4}**	5.8864×10^{-2}	9.9691×10^{-4}	9.8253×10^{-4}	9.82487×10^{-4}	9.8249×10^{-4}	9.82511×10^{-4}	9.8257×10^{-4}	9.83606×10^{-4}	9.8464×10^{-4}	9.8423×10^{-4}	1.6600×10^{-3}	3.6040×10^{-1}
Mean	**9.82473×10^{-4}**	6.5348×10^{-2}	1.6541×10^{-3}	9.8331×10^{-4}	9.8315×10^{-4}	9.8250×10^{-4}	9.8356×10^{-4}	9.8258×10^{-4}	9.83606×10^{-4}	9.8651×10^{-4}	9.8561×10^{-4}	1.7463×10^{-3}	3.6497×10^{-1}
Max	**9.82473×10^{-4}**	8.9472×10^{-2}	1.9845×10^{-3}	1.8476×10^{-3}	9.8324×10^{-4}	9.8261×10^{-4}	9.8412×10^{-4}	9.8264×10^{-4}	9.83606×10^{-4}	9.8741×10^{-4}	9.8562×10^{-4}	1.9476×10^{-3}	1.0010
TDM													
Min	**9.807313×10^{-4}**	9.84385×10^{-4}	9.81148×10^{-4}	9.8203×10^{-4}	9.80751×10^{-4}	9.8033×10^{-4}	9.81064×10^{-4}	9.8204×10^{-4}	9.81232×10^{-4}	9.8249×10^{-4}	9.81754×10^{-4}	9.8247×10^{-4}	1.0531×10^{-3}
Mean	**9.80751×10^{-4}**	9.8654×10^{-4}	9.8254×10^{-4}	9.8206×10^{-4}	9.8077×10^{-4}	9.8034×10^{-4}	9.8106×10^{-4}	9.8379×10^{-4}	9.8461×10^{-4}	9.8264×10^{-4}	9.8652×10^{-4}	9.8364×10^{-4}	1.8496×10^{-3}
Max	**9.8080×10^{-4}**	1.5467×10^{-3}	9.8252×10^{-4}	9.8208×10^{-4}	9.8100×10^{-4}	9.8036×10^{-4}	9.8106×10^{-4}	9.8997×10^{-4}	9.8514×10^{-4}	9.8401×10^{-4}	9.9546×10^{-4}	9.9431×10^{-4}	2.6478×10^{-3}

two-diode, and three-diode models. It should be noted that the three-diode model yields a lower relative error value compared to the single-diode and two-diode models, making it a more accurate model.

Table 10 presents the values of 5 unknown parameters of the PWP201 solar module's single-diode model, obtained through the BDGOA algorithm and 14 other algorithms. To ensure a comprehensive and fair comparison, additional methods such as JAYA [60], simplified teaching–learning-based optimization algorithm (STLBO) [61], teaching–learning-based artificial bee colony (TLABC) [62], comprehensive learning particle swarm optimizer (CLPSO) [63], biogeography-based learning particle swarm optimization (BLPSO) [64], and DE/BBO [47] are also utilized. By examining Table 10 and comparing it with Table 5, it becomes evident that only the WHHO and SWOA methods achieved the lowest RMSE value as before. Furthermore, the STLBO and TLABC algorithms successfully attained a lower optimal value. Another crucial aspect to consider when comparing algorithms is their convergence speed. Figure 11 graphically depicts the convergence speed of the algorithms over 5000 iterations. From this figure, it becomes apparent that the proposed method not only achieved the lowest RMSE value but also exhibited a faster convergence rate compared to other algorithms.

Among the various algorithms, the most efficient one demonstrates commendable performance when dealing with a large number of unknown system parameters. Consequently, the two-diode and three-diode models are implemented to allow for a more meticulous examination of the algorithms (Tables 11 and 12). As clearly indicated in Tables 11 and 12, algorithms that successfully attained the lowest RMSE value in the single-diode model, such as the BDGOA algorithm, failed to showcase satisfactory performance as the number of unknown parameters increased. Figures 12 and 13 illustrate the convergence speed of the algorithms in the two-diode and three-diode models. These figures highlight the superior convergence speed of the BDGOA algorithm. However, it is worth noting that the GOA algorithm exhibited better performance in the PWP201 system when compared to RTC France.

Another important factor is the robustness and stability of the algorithms. To assess this, each algorithm was executed 30 times, and the results are presented in Table 13. Based on this table, the BDGOA algorithm demonstrated exceptional performance, particularly in the single-diode model. The SWOA and WHHO algorithms also displayed considerable stability in comparison to other algorithms.

4.3 | Experimental study

This section provides a discussion on the SM55, KC200GT, and SW255 solar modules, with their parameters identified through the BDGOA algorithm. Initially, the unknown parameters of these modules are determined under the condition's of 1000 W/m^2 irradiance and 25°C as presented in Table 14. Subsequently, Equations (11) and (12) are utilized to analyse the behaviour of the identified model while considering varia-

TABLE 9 Relative error for each measurement.

			SDM		DDM		TDM	
DATA	V_L (V)	I_L (A)	I_{te} (A)	R_{err}	I_{te} (A)	R_{err}	I_{te} (A)	R_{err}
1	0.1248	1.0315	1.029122	0.002310	1.029153	0.002280	1.029001	0.002428
2	1.8093	1.0300	1.027384	0.002545	1.027354	0.002575	1.028312	0.001641
3	3.3511	1.0260	1.025742	0.000251	1.025791	0.000203	1.025961	0.000038
4	4.7622	1.0220	1.024104	−0.002054	1.024156	−0.002105	1.023910	−0.001865
5	6.0538	1.0180	1.022283	−0.004189	1.022276	−0.004182	1.020215	−0.002171
6	7.2364	1.0155	1.0199172	−0.004330	1.0199148	−0.004328	1.019215	−0.003644
7	8.3189	1.0140	1.016350	−0.002312	1.016384	−0.002345	1.016323	−0.002285
8	9.3097	1.0100	1.010491	−0.000486	1.010494	−0.000488	1.010401	−0.000396
9	10.2163	1.0035	1.000678	0.002819	1.000664	0.002834	1.000541	0.002957
10	11.0449	0.9880	0.984653	0.003398	0.984634	0.003418	0.984934	0.003112
11	11.8018	0.9630	0.959697	0.003441	0.959612	0.003530	0.959612	0.003530
12	12.4929	0.9255	0.923048	0.002655	0.923013	0.002694	0.924913	0.000634
13	13.1231	0.8725	0.872588	−0.00010	0.872516	−0.000018	0.872523	−0.000026
14	13.6983	0.8075	0.807310	0.000235	0.807318	0.000225	0.807312	0.000232
15	14.2221	0.7265	0.727957	−0.002002	0.727954	−0.001997	0.727264	−0.001050
16	14.6995	0.6345	0.636466	−0.003089	0.636421	−0.003018	0.636031	−0.002407
17	15.1346	0.5345	0.535696	−0.002232	0.535631	−0.002111	0.535534	−0.001930
18	15.5311	0.4275	0.428816	−0.003069	0.428804	−0.003041	0.428634	−0.002645
19	15.8929	0.3185	0.318668	−0.000529	0.318640	−0.000439	0.318614	−0.000357
20	16.2229	0.2085	0.207857	0.003093	0.207830	0.003223	0.207931	0.002736
21	16.5241	0.1010	0.098354	0.026901	0.098380	0.026631	0.098997	0.020232
22	16.7987	−0.0080	−0.008169	−0.020733	−0.008192	−0.023437	−0.008100	−0.012345
23	17.0499	−0.1110	−0.110968	0.000284	−0.110927	0.000658	−0.110961	0.000351
24	17.2793	−0.2090	−0.209117	−0.000562	−0.209126	−0.000602	−0.209101	−0.000483
25	17.4885	−0.3030	−0.302022	0.003237	−0.302011	0.003274	−0.302831	0.000558

TABLE 10 Detailed results for SDM of PWP201.

Algorithm	I_{ph} (A)	I_{sd1} (μA)	R_s (Ω)	R_{sh} (Ω)	n_1	RMSE
BDGOA	**1.03051**	**3.48210**	**1.20127**	**981.905230**	**1.34998**	$\mathbf{2.425074 \times 10^{-3}}$
GOA	1.03392	2.48316	1.23163	634.57970	1.31518	2.64345×10^{-3}
FPSO	1.03061	3.45162	1.20206	966.77093	1.34906	2.42525×10^{-3}
WHHO	1.03051	3.48210	1.20127	981.90523	1.34998	2.42507×10^{-3}
EHHO	1.03058	3.45996	1.20185	971.27602	1.34931	2.42516×10^{-3}
SWOA	1.03051	3.48221	1.20127	981.96750	1.34999	2.42507×10^{-3}
CWOA	1.03164	3.09598	1.21219	827.54687	1.33768	2.45168×10^{-3}
WOA	1.03393	2.49034	1.23192	644.59884	1.31542	2.63576×10^{-3}
RGWO	1.03165	3.12486	1.21082	829.35431	1.33865	2.44998×10^{-3}
JAYA	1.0307	3.4931	1.2014	1000	1.3514	2.42778×10^{-3}
STLBO	1.0305	3.4824	1.2013	982.0387	1.3511	2.42507×10^{-3}
TLABC	1.0305	3.4826	1.2013	982.1815	1.3512	2.42507×10^{-3}
CLPSO	1.0304	3.6131	1.1978	1000	1.3551	2.42806×10^{-3}
BLPSO	1.0305	3.5176	1.2002	992.7901	1.3522	2.42523×10^{-3}
DE/BBO	1.0303	3.6172	1.1969	1000	1.3552	2.42825×10^{-3}

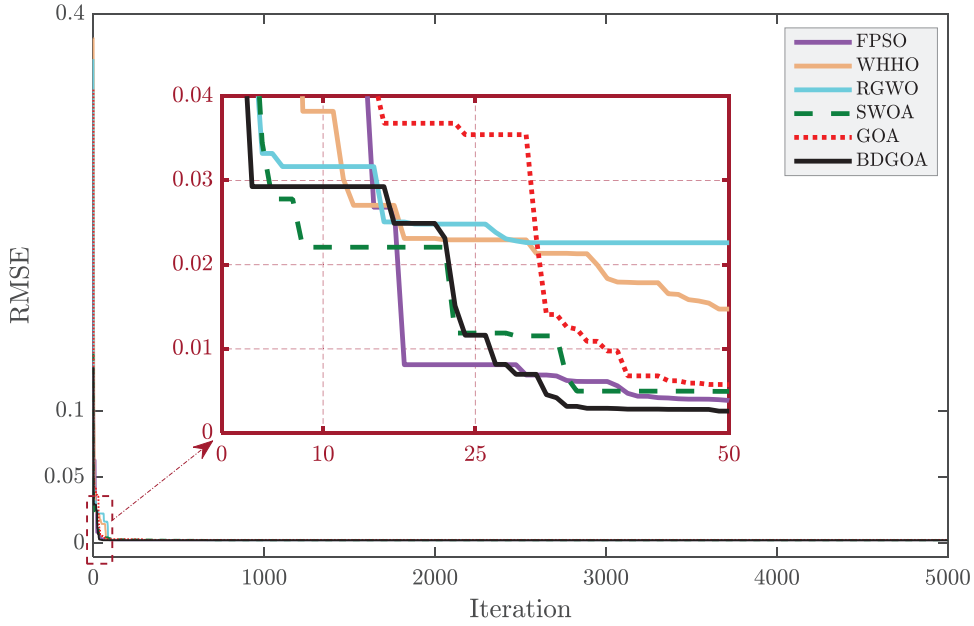

FIGURE 11 RMSE evolution of the algorithms for the SDM.

TABLE 11 Detailed results for DDM of PWP201.

Algorithm	I_{ph} (A)	I_{sd1} (μA)	I_{sd2} (μA)	R_s (Ω)	R_{sh} (Ω)	n_1	n_2	RMSE
BDGOA	**1.03238**	**2.49291**	**1.00005**	**1.23018**	**745.71538**	**1.30530**	**1.31193**	**2.04453×10^{-3}**
GOA	1.03058	5.0000	2.91745	1.20717	1000	2	1.03058	2.48115×10^{-3}
FPSO	1.03060	2.4101	2.82452	1.20776	1000	1.94700	1.33105	2.48750×10^{-3}
WHHO	1.032381	2.51291	1.00005	1.23928	744.71538	1.31730	1.31693	2.04653×10^{-3}
EHHO	1.032341	2.67581	1.52821	1.23313	715.45241	1.54974	1.28392	2.2137×10^{-3}
SWOA	1.031434	2.63811	1.0001	1.23563	821.6525	1.32099	2.77788	2.0530×10^{-3}
CWOA	1.0332	2.6759	1.52820	1.23312	715.4537	1.5499	1.2844	2.2137×10^{-3}
WOA	1.0323	2.5129	1.0000	1.2392	744.7153	1.3173	1.3173	2.0465×10^{-3}
RGWO	1.03058	2.5126	2.91745	1.20717	1000	2	1.33376	2.48115×10^{-3}
JAYA	1.0326	2.6896	4.1973	1.2240	748.3831	1.3234	2.3680	2.2178×10^{-3}
STLBO	1.0328	2.5708	1.6899	1.2137	712.2977	1.3218	1.7314	2.2785×10^{-3}
TLABC	1.0331	2.6762	1.5280	1.2334	715.4478	1.5499	1.2832	2.2138×10^{-3}
CLPSO	1.0291	0.0010	9.3813	0.0314	75.6531	1.0000	1.5755	3.3925×10^{-3}
BLPSO	1.0265	9.2998	2.2586×10^{-2}	0.0301	1000	1.5225	1.4164	3.7559×10^{-3}
DE/BBO	1.0318	0.32774	2.4306×10^{-6}	1.2061	845.2495	1.3443	1.3443	2.400×10^{-3}

tions in temperature and irradiance. This investigation involves experimentation with different temperatures and irradiances.

Figures 14, 15, and 16 correspond to the SM55, KC200GT, and SW255 modules, respectively. These figures demonstrate that the behaviour of the experimental and identified models closely resemble each other, with a negligible level of error that is inconsequential in engineering. Thus, the accuracy of the parameters derived from the BDGOA algorithm is convincingly established. These figures also illustrate that as the level of irradiance decreases, the current produced by the solar module diminishes, consequently resulting in a decline in output power.

Figures 17 and 18 showcase the impact of temperature on the SM55 and KC200GT modules, respectively. These figures further substantiate the precision and accuracy of the parameters identified by the BDGOA algorithm, as the behaviour of the identified model closely aligns with that of the experimental model. Notably, these figures elucidate that an increase in the temperature of the solar cells leads to an increase in ohmic resistance, subsequently causing a decline in current.

TABLE 12 Detailed results for TDM of PWP201.

Algorithm	I_{ph} (A)	I_{sd1} (μA)	I_{sd2} (μA)	I_{sd3} (μA)	R_s (Ω)	R_{sh} (Ω)	n_1	n_2	n_3	RMSE
BDGOA	**1.02011**	**3.48214**	**1.01001**	**1.03000**	**1.15021**	**975.86961**	**1.39763**	**1.86704**	**2**	$\mathbf{2.0099 \times 10^{-3}}$
GOA	1.04322	6.64271	9.68379	1.00000×10^{-6}	1	511.90787	1.94553	1.47606	1.99998	7.83812×10^{-3}
FPSO	1.03039	1.00000×10^{-3}	3.51253	1.00000×10^{-6}	1.20053	1000	2	1.35090	1.95841	2.42530×10^{-3}
WHHO	1.030514	3.48214×10^{-6}	1.000010×10^{-6}	1.000000×10^{-6}	1.200216	981.86961	1.39763	1.86704	2	2.0166×10^{-3}
EHHO	1.030571	3.439412	5.361479×10^{-5}	5.36524×10^{-3}	1.210242	991.362145	1.40361	1.40371	1.59847	2.4249×10^{-3}
SWOA	1.0305	3.4822×10^{-6}	1.0000×10^{-6}	1.0000×10^{-6}	1.2012	981.9781	1.4029	1.8671	2	2.0166×10^{-3}
CWOA	1.0305	3.4788	7.2209×10^{-5}	7.9930×10^{-2}	1.2005	992.7808	1.4032	1.9996	1.6487	2.4250×10^{-3}
WOA	1.0270	3.9028	2.0334×10^{-4}	6.0996×10^{-2}	1.1910	966.4183	1.4157	1.9992	1.6278	2.5814×10^{-3}
RGWO	1.030514	1	1.47299	1.00936	1.20126	982.02536	1.34999	1.34999	1.34999	2.42507×10^{-3}
JAYA	1.0263	2.4380	8.4019	2.4413×10^{-1}	1.1911	710.7260	1.3885	1.8790	1.3544	2.7525×10^{-3}
STLBO	1.0327	0	5.3435	2.4748	1.1448	1000	1.8457	1.4547	1.9590	3.4186×10^{-3}
TLABC	1.0264	9.1106	2.0912×10^{-2}	6.3249×10^{-2}	1.0869	602.9147	1.5220	1.3011	1.5370	3.7258×10^{-3}
CLPSO	1.0419	3.43995	6.6266×10^{-7}	35.1499	1	755.0178	1.9938	1.2982	1.9987	9.9858×10^{-3}
BLPSO	1.0344	4.7853	1.16444	2.6812×10^{-3}	1	1000	2	1.5566	2	6.3626×10^{-3}
DE/BBO	1.0307	0	3.2036	3.1737	1.1952	996.3251	1.7749	1.3965	1.9564	2.4916×10^{-3}

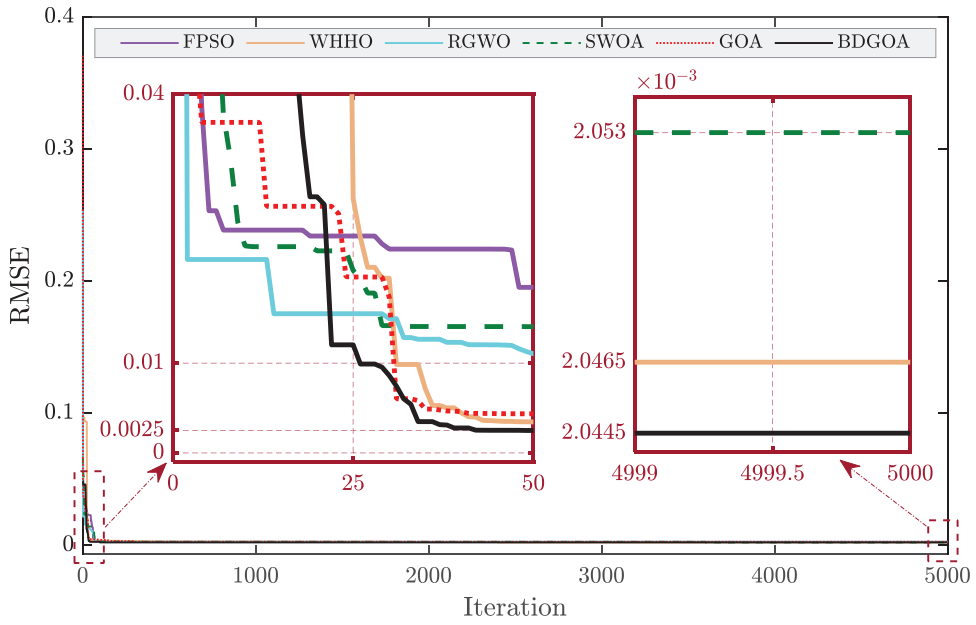

FIGURE 12 RMSE evolution of the algorithms for the DDM.

4.4 | The effects of the temperature and irradiance on the module parameters

In this section, an investigation is undertaken to analyse the impact of temperature and irradiance on the parameters of the mathematical model of the solar cell. The preceding section has already established the direct relationship between irradiance and the current generated by the solar cell, as well as the inverse relationship between temperature and current. This correlation is once again reaffirmed by the findings presented in Tables 15 and 16. Table 15 clearly illustrates that while the temperature remains constant at 25°C, an increase in irradiance results in a corresponding increase in the current source (I_{ph}), while the shunt resistance (R_{sh}), series resistance (R_s), and the diode ideality factor (n_1) remain relatively stable. It is important to note that the reverse saturation current (I_{sd1}) of the diode exhibits a direct relationship with temperature, leading to an augmented absorption of photons as temperature rises. Consequently, the value of I_{sd1} also increases, as indicated in Table 16.

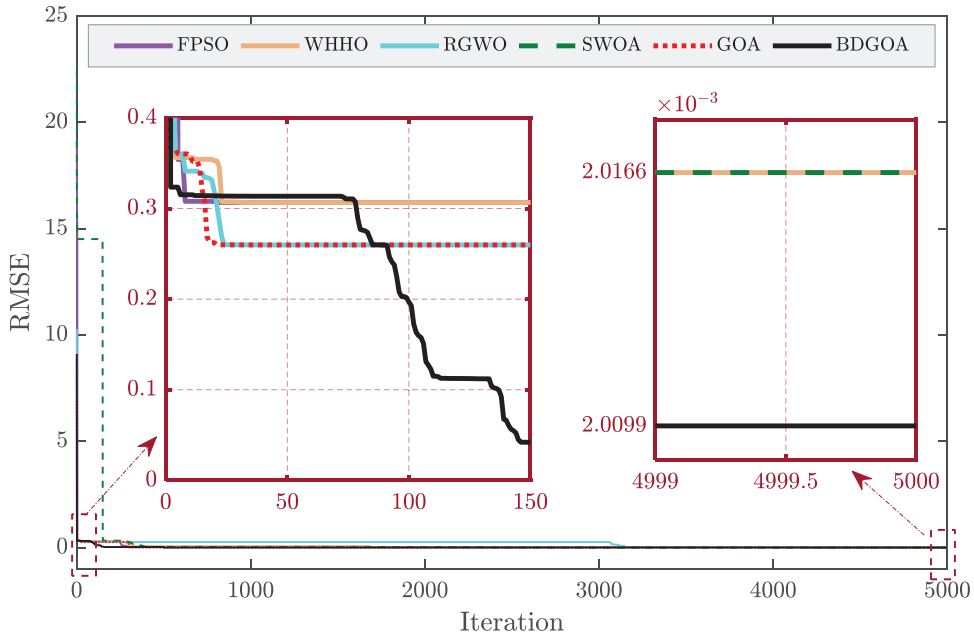

FIGURE 13 RMSE evolution of the algorithms for the TDM.

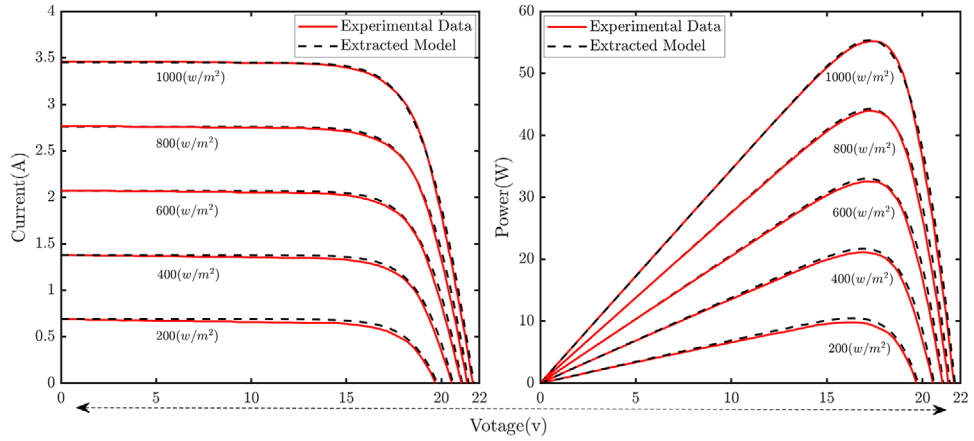

FIGURE 14 Evaluation of the characteristics of SM55 module for the parameters estimated by the proposed algorithm in comparison with those provided by the manufacturer under irradiance changes at constant $T = 25$ °C.

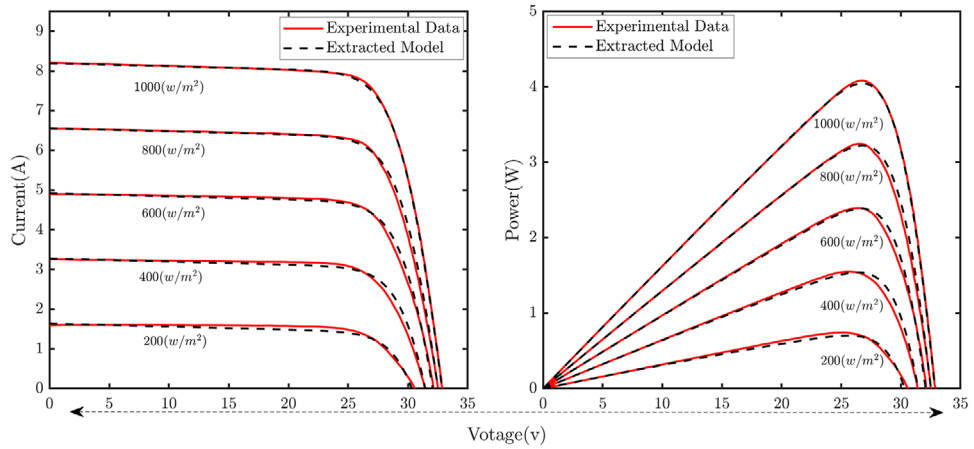

FIGURE 15 Evaluation of the characteristics of KC200GT module for the parameters estimated by the proposed algorithm in comparison with those provided by the manufacturer under irradiance changes at constant $T = 25$ °C.

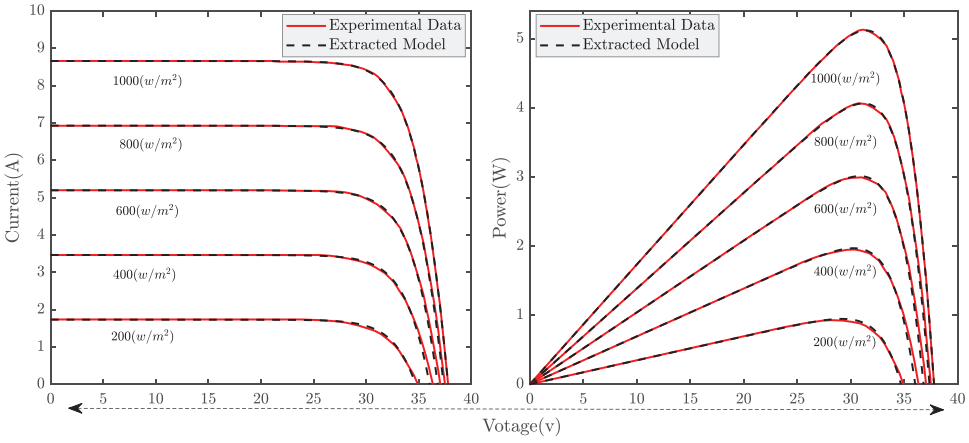

FIGURE 16 Evaluation of the characteristics of SW255 module for the parameters estimated by the proposed algorithm in comparison with those provided by the manufacturer under irradiance changes at constant $T = 25$ °C.

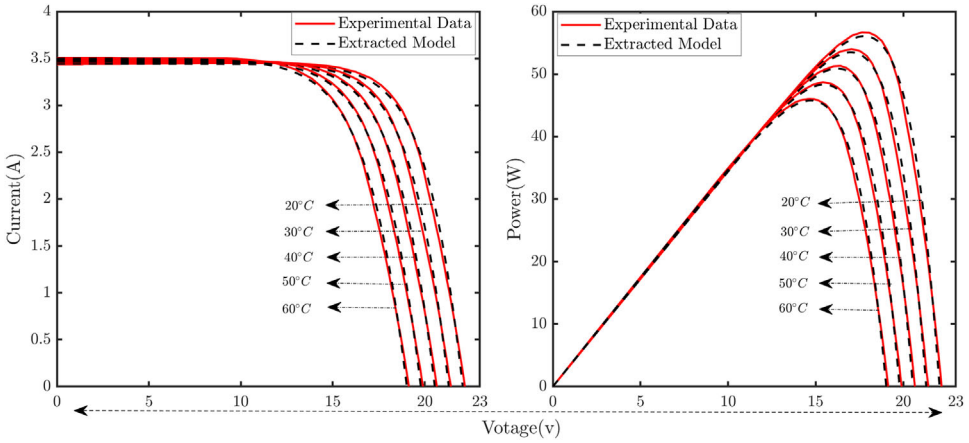

FIGURE 17 Evaluation of the characteristics of SM55 module for the parameters estimated by the proposed algorithm in comparison with those provided by the manufacturer under temperature changes at constant irradiance $G = 1000$ w/m^2.

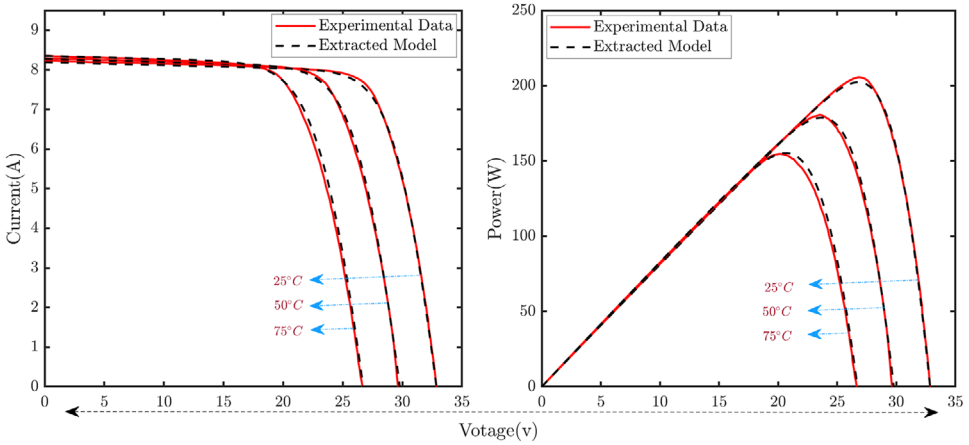

FIGURE 18 Evaluation of the characteristics of KC200GT module for the parameters estimated by the proposed algorithm in comparison with those provided by the manufacturer under temperature changes at constant irradiance $G = 1000$ w/m^2.

TABLE 13 Comparison between RMSE value for the SDM, DDM, TDM of PWP201 obtained by different methods after 30 runs.

	SDM							
Algorithm	**BDGOA**	**GOA**	**FPSO**	**WHHO**	**EHHO**	**SWOA**	**CWOA**	**WOA**	**RGWO**
Min	$\mathbf{2.425074 \times 10^{-3}}$	2.64345×10^{-3}	2.42525×10^{-3}	2.42507×10^{-3}	2.42516×10^{-3}	2.42507×10^{-3}	2.45168×10^{-3}	2.63576×10^{-3}	2.44998×10^{-3}
Mean	$\mathbf{2.425074 \times 10^{-3}}$	5.6147×10^{-3}	2.4252×10^{-3}	2.42510×10^{-3}	2.425669×10^{-3}	2.42507×10^{-3}	2.4678×10^{-3}	2.8476×10^{-3}	2.4597×10^{-3}
Max	$\mathbf{2.425074 \times 10^{-3}}$	6.1478×10^{-3}	2.4252×10^{-3}	2.4253×10^{-3}	2.43125×10^{-3}	2.42507×10^{-3}	2.7864×10^{-3}	3.1647×10^{-3}	2.4949×10^{-3}
				DDM					
Min	$\mathbf{2.04453 \times 10^{-3}}$	2.48115×10^{-3}	2.48750×10^{-3}	2.04653×10^{-3}	2.2137×10^{-3}	2.0530×10^{-3}	2.2137×10^{-3}	2.0465×10^{-3}	2.48115×10^{-3}
Mean	$\mathbf{2.0450 \times 10^{-3}}$	4.5987×10^{-3}	2.4895×10^{-3}	2.04887×10^{-3}	2.2264×10^{-3}	2.05464×10^{-3}	2.2647×10^{-3}	2.04774×10^{-3}	2.4889×10^{-3}
Max	$\mathbf{2.04551 \times 10^{-3}}$	8.3647×10^{-3}	2.4899×10^{-3}	2.5631×10^{-3}	3.1547×10^{-3}	2.05510×10^{-3}	2.8564×10^{-3}	2.4946×10^{-3}	2.4898×10^{-3}
				TDM					
Min	$\mathbf{2.0099 \times 10^{-3}}$	7.83812×10^{-3}	2.42530×10^{-3}	2.0166×10^{-3}	2.4249×10^{-3}	2.0166×10^{-3}	2.4250×10^{-3}	2.5814×10^{-3}	2.42507×10^{-3}
Mean	$\mathbf{2.0154 \times 10^{-3}}$	2.3478×10^{-2}	2.4261×10^{-3}	2.02164×10^{-3}	2.4316×10^{-3}	2.02146×10^{-3}	2.4251×10^{-3}	2.6154×10^{-3}	2.4251×10^{-3}
Max	$\mathbf{2.0166 \times 10^{-3}}$	4.8479×10^{-2}	2.4264×10^{-3}	2.03464×10^{-3}	2.4431×10^{-3}	2.06461×10^{-3}	2.4374×10^{-3}	2.8461×10^{-3}	$2.4262 \times 10{-3}$

Furthermore, it should be emphasized that series resistance value (R_s) consistently falls below 0.4, which confirms that the series resistance value for monocrystalline modules is always less than 0.4. Moreover, this serves as evidence that the ideal coefficient of the diode, represented by n_1, varies across different modules. For instance, the KC200GT module, being of the emission type, demonstrates an ideal coefficient of n that is nearly equal to 1.

4.5 | The impact of BDGOA parameters in finding global minima

The BDGOA method, an enhancement of the classic GOA method, features parameters categorized into two groups: GOA parameters and those specific to the elimination and search space control phases. While the impact of GOA parameters is detailed in the reference article [], this section focuses exclusively on the parameters unique to the proposed BDGOA method. As elaborated in Section 3, the BDGOA method introduces four additional parameters (ep, et, Th, w) beyond those in the GOA method.

4.5.1 | The impact of *ep* and *et* parameters on the performance of the proposed method

In the BDGOA method, the parameters ep and et are utilized during the elimination phase. The ep parameter allows for the selection and removal of a percentage of locusts, which are then replaced by new locusts distributed randomly in new areas. The et parameter determines the frequency of entering the elimination phase during the execution of the BDGOA algorithm. It is important to note that both the number of repetitions and the total number of locusts remain constant.

In the first test, we initially increase the value of ep from 5 to 15 and subsequently to 30. As illustrated in Figure 19, the convergence speed increases with the rise in ep up to iteration 100. This is because, in each repetition of et, new locusts are generated and must explore new areas. However, beyond 100 iterations, it is observed that at ($ep = 30$), the algorithm's speed decreases, and the convergence process slows down. This indicates that setting the BDGOA algorithm parameter to an optimal value not only enhances convergence speed but also ensures high resistance and stability.

In the second test, we aim to demonstrate the effect of the (et) parameter. To this end, we increase its value from 2 to 10 and subsequently to 20. As illustrated in Figure 20, the convergence speed increases with the rise in (et). When (et) is set to 2, the BDGOA algorithm enters the elimination loop 2500 times. This increases the time required for the BDGOA algorithm to reach the local minimum value, thereby enhancing its resistance. Consequently, its speed is lower compared to when (et) is set to 20, where the proposed algorithm enters the elimination loop 250 times.

TABLE 14 Parameters of the three PV modules identified by the BDGOA method at STC.

Parameters	SM55	KC200GT	SW255
I_{ph} (A)	3.470862355052374	8.218606016677501	1.746816958876764
I_{sd1} (μA)	$2.377347964254658 \times 10^{-4}$	0.001436006218871	0.033178077675460
R_s (Ω)	0.517851206414101	0.240939897541895	0.388661039315355
R_{sh} (Ω)	$3.437859816584798 \times 10^{2}$	$1.302813825145347 \times 10^{2}$	1000
n_1	1	1.055285597003159	1.274607310967329
RMSE	**0.021139045580187**	**0.028213640103146**	**0.009995405934055**

TABLE 15 Optimal estimated parameters by BDGOA for three types of PV modules at different irradiance (G) and constant temperature of $T = 25$ °C.

Parameters	SM55	KC200GT	SW255
***G* = 200**			
I_{ph} (A)	0.686487860691327	1.608849831906320	1.746816956890225
I_{sd1} (μA)	0.021776669813637	$4.852657050051957 \times 10^{-4}$	0.033177979993694
R_s (Ω)	0.309322025760319	1.106179645946718	0.388661359866792
R_{sh} (Ω)	$3.495675285194748 \times 10^{2}$	$9.131700850440784 \times 10^{2}$	1000
n_1	1.0237567291785018	1.006454970099246	1.274607100447143
RMSE	**0.002025079253808**	**0.007764938321150**	**0.009995405934055**
***G* = 400**			
I_{ph} (A)	1.384033025830558	3.255412634852096	3.476994320252256
I_{sd1} (μA)	$3.051743640265893 \times 10^{-4}$	0.007753541433883	0.020786558856430
R_s (Ω)	0.712761861228674	0.435509390397835	0.256109285950023
R_{sh} (Ω)	$3.393632090216943 \times 10^{2}$	$1.374660175622723 \times 10^{2}$	1000
n_1	1	1.1041831819295220	1.245141664726922
RMSE	**0.006253256699189**	**0.013226377079533**	**0.012747582066599**
***G* = 600**			
I_{ph} (A)	2.079263990458108	4.890653933053618	5.208789869584503
I_{sd1} (μA)	$2.717710751312673 \times 10^{-4}$	0.064768884306755	0.009040276793170
R_s (Ω)	0.335775424901300	0.270615139088943	0.201092803443840
R_{sh} (Ω)	$3.475813467257393 \times 10^{2}$	$4.015119133755529 \times 10^{2}$	1000
n_1	1	1.1079060573832047	1.191102524780014
RMSE	**0.009558001210683**	**0.040284398923021**	**0.017904967465303**
***G* = 800**			
I_{ph} (A)	2.777408861767876	6.558134730355183	6.937368054277113
I_{sd1} (μA)	$4.498116763197091 \times 10^{-4}$	$4.236775162053583 \times 10^{-4}$	0.012433492224247
R_s (Ω)	0.331638687515754	0.327253547120007	0.149356393058151
R_{sh} (Ω)	$3.360266607657530 \times 10^{2}$	$1.480320416373675 \times 10^{2}$	1000
n_1	1.024161273927083	1	1.206986081180923
RMSE	**0.011353604434747**	**0.027582435865512**	**0.025115175835126**
***G* = 1000**			
I_{ph} (A)	3.470862355052374	8.218606016677501	8.672901235
I_{sd1} (μA)	$2.377347964254658 \times 10^{-4}$	0.001436006218871	0.0164600397
R_s (Ω)	0.417851206414101	0.240939897541895	0.1221941067
R_{sh} (Ω)	$3.437859816584798 \times 10^{2}$	$1.302813825145347 \times 10^{2}$	925.14731112
n_1	1	1.055285597003159	1.214607310967329
RMSE	**0.021139045580187**	**0.028213640103146**	**0.009995405934055**

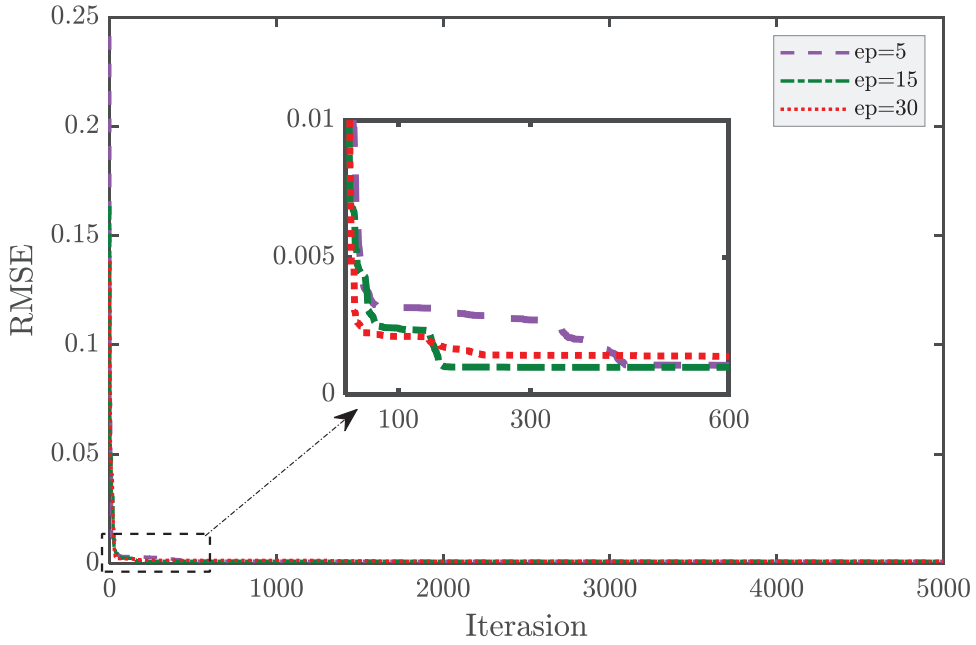

FIGURE 19 The impact of ep parameter on the performance of BDGOA algorithm ($L = 5000, et = 50, w = 0.5$).

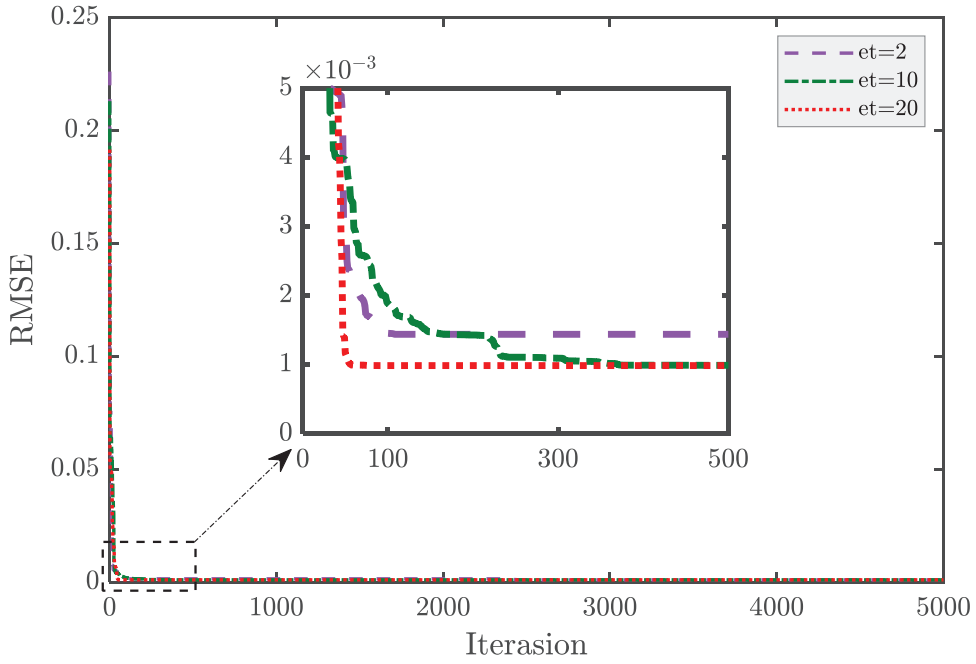

FIGURE 20 The impact of et parameter on the performance of BDGOA algorithm ($L = 5000, ep = 15, w = 0.5$).

4.5.2 | The effect of *Th* and *w* parameters on the performance of the proposed method

The parameters *Th* and *w* are utilized to control the search space. As detailed in Section 3, the *Th* parameter is reduced to prevent locusts from leaving the search space, while the *w* parameter is used to enlarge the search space. The search in each iteration occurs at the rate *w*.

As illustrated in Figure 21, decreasing the value of the *w* parameter slows down the convergence speed because the search space expands at a slower rate until it reaches its total value. Consequently, locusts need more time to explore the entire state space. However, it is important to note that although the convergence speed decreases, the algorithm's resistance increases, preventing it from getting stuck in local minima.

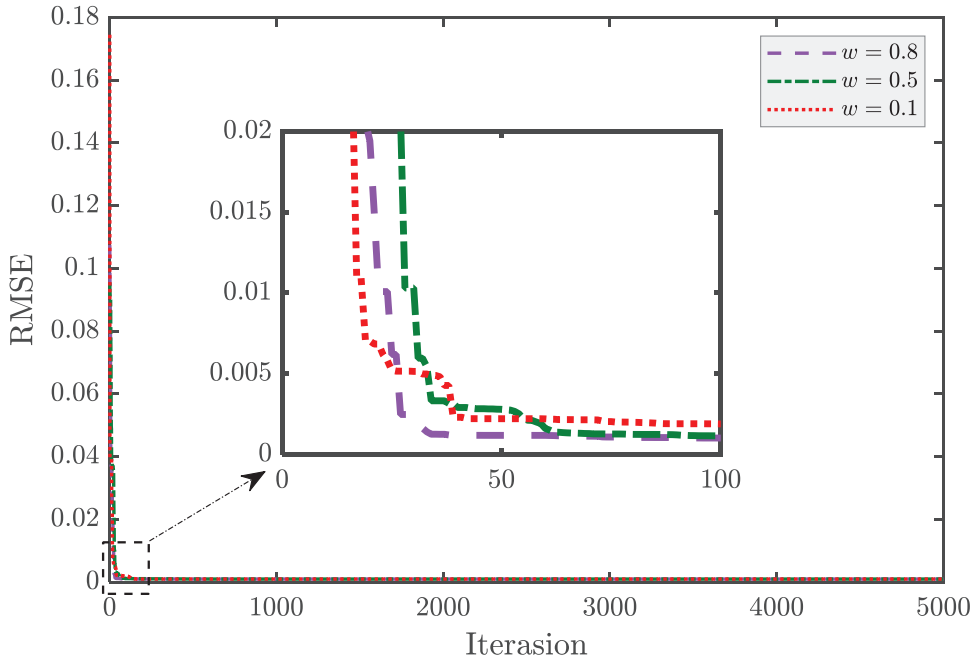

FIGURE 21 The impact of w parameter on the performance of BDGOA algorithm ($L = 5000$, $ep = 15$, $et = 50$).

4.6 | The impact of solar cell parameter identification in industry and economy

Identifying solar cell parameters has a profound impact on the industry, economy, and cost savings in operational and maintenance costs for solar PV systems. Accurately identifying and optimizing the efficiency of solar cells allows manufacturers to produce more effective solar panels, leading to higher energy output from the same amount of sunlight. This makes solar technology more competitive with traditional energy sources, reducing the cost per watt of solar energy and making it more affordable for consumers and businesses. This can drive increased adoption of solar technology, fostering growth in the renewable energy sector and creating jobs. Higher efficiency panels require fewer installations to achieve the same energy output, reducing installation and maintenance costs, and resulting in less frequent replacements and lower operational costs over the lifespan of the system.

Understanding the temperature coefficient helps in designing solar panels that perform better under varying environmental conditions, ensuring that solar panels maintain their efficiency even in high-temperature regions. This enhances their reliability and lifespan, making solar investments more attractive and encouraging more widespread use. Panels with optimized temperature coefficients require less maintenance and have longer lifespans, reducing operational costs and contributing to energy cost savings. Panels with a lower temperature coefficient experience less efficiency loss in high temperatures, leading to more consistent energy production and lower cooling costs. This reduces the need for additional cooling systems and maintenance, further lowering operational expenses. These improvements not only enhance the performance and reliability of solar panels but also make solar energy a more viable and cost-effective option, promoting its adoption and supporting the transition to sustainable energy sources.

5 | CONCLUSIONS

Overall, the bio-dynamics grasshopper optimization algorithm (BDGOA) proposed in this paper demonstrated significant improvements over the original GOA algorithm, including higher convergence speed, enhanced global exploration, and increased robustness. Extensive experiments and comparisons with existing methods validated the performance of the BDGOA algorithm, showing a close match with experimental data for PV cell and module models. The algorithm effectively estimated parameters for various commercial modules under varying temperature and irradiance conditions. Notably, the saturation current of the diode and the photocurrent exhibited slight variations with temperature and irradiance changes, while other parameters remained consistent across different operating conditions. These findings underscore the high performance and accuracy of the proposed algorithm, paving the way for its practical application in PV modelling and optimization. Additionally, the impact of BDGOA algorithm parameters on convergence speed and the ability to escape local minima was analysed. Finally, the significance of accurately identifying solar cell parameters in the industry and the resulting cost savings was highlighted.

TABLE 16 Optimal estimated parameters by BDGOA for three modules at different temperature values and constant irradiance of $G = 1000$ w/m^2.

PV Modules	Temperature	I_{ph} (A)	I_{sd1} (μA)	R_s (Ω)	R_{sh} (Ω)	n_1	RMSE
	20°C	3.449518230759574	$5.553901054807567 \times 10^{-4}$	0.510855281158646	435.3647	1.081563454730112	**0.017523039512058**
	30°C	3.44440365830375	0.008533509212041 48	0.483869439343906	432.254482733995	1.148700262121470	**0.021008871303678**
SM55	40°C	3.439524671665240	1.001825872374 14	0.452871171904451	466.707521042000	1.307318212858 00	**0.016835490992136**
	50°C	3.437399330127881	0.090229449857 3636	0.487226772844036	330.637321258794	1.136287689557 45	**0.017896881918109**
	60°C	3.432524827019689	1.001773881993 84	0.452872666075687	466.665524838221	1.228796428964059	**0.016835490988922**
	25°C	8.218606016677501	0.001436006218871	0.240939897541895	$1.302813825145347 \times 10^2$	1.159202318396120	**0.028213640103146**
KC200GT	50°C	8.208941151751097	3.773615282717802	0.158259528938871	$3.217451863214721 \times 10^2$	1.465080937146778	**0.082797442165082**
	75°C	8.201344972976629	3.559084696673 06	0.253324042473312	246.044561264732	1.309327303043582	**0.046835159602920**

NOMENCLATURE

R_s	Series resistance
R_{sh}	Shunt resistance
I_{ph}	Current source
I_t	Output current
I_d	Diode current
I_{sh}	Shunt resistance current
I_{sd}	Diode reverse saturation current
V_t	Terminal voltage
n	The diode ideality factor
q	The magnitude of charge on an electron (1.602×10^{-19})
k	The Boltzmann constant (1.381×10^{-23} (J/K))
T	The cell temperature (K)
g	Constant of gravity
u	Constant drift
$\hat{e}_g$	Unity vector towards earth center
$\hat{e}_w$	Unity vector in the wind direction
N	The number of grasshoppers
ub_d	The upper bound in the dth dimension of $s(r)$
lb_d	The lower bound in the dth dimension of $s(r)$
L	The maximum number of iterations
ep	Elimination percent
et	Elimination iteration
θ	Vector of unknown parameters
N_P	Number of solar cells in parallel
N_s	The number of solar cells in series
I_{ph_STC}	Light generated current at STC ($T_{STC} = 25°C$)
G	The surface irradiance of the cell
G_{STC}	The irradiance at STC (1000 w/m^2)
K_i	The short-circuit current coefficient
K_v	Open circuit voltage coefficient
N_E	The number of measured data
S_i	The social interaction
G_i	The gravity force on the grasshopper
A_i	Wind advection
d_{ij}	The distance between ith and jth grasshopper
$\hat{d}_{ij}$	An unit vector from ith to jth grasshopper
$s(r)$	The social forces strength
l	The attractive length scale
f	The attraction intensity
T_d	Value of the dth dimension in the target
c_{max}	The maximum value of c
c_{min}	The minimum value of c
Th	Percentage of the problem domain
w	[0,1]

AUTHOR CONTRIBUTIONS

Mostafa Jabari: Methodology; resources; software; writing—original draft; writing—review & editing. **Amin Rad**: Data curation; project administration; resources; software. **Morteza Azimi Nasab**: Data curation; supervision; writing—original draft; writing—review & editing. **Mohammad Zand**: Data curation; methodology; software; writing—original draft.

Sanjeevikumar Padmanaban: Writing—original draft; writing—review & editing. **S. M. Muyeen**: Data curation; methodology; software; supervision. **Josep M. Guerrero**: Writing—original draft; writing—review & editing.

ACKNOWLEDGEMENTS

Qatar National Library Open Access publishing facilitated by the Qatar National Library, as part of the Wiley Qatar National Library agreement.

Open access funding provided by the Qatar National Library.

CONFLICT OF INTEREST STATEMENT

The authors declare no conflicts of interest.

DATA AVAILABILITY STATEMENT

Data are available by request to the corresponding author Prof. S. M. Muyeen (sm.muyeen@qu.edu.qa)

ORCID

Mostafa Jabari https://orcid.org/0000-0003-2169-9802
Morteza Azimi Nasab https://orcid.org/0000-0002-5145-0429
Mohammad Zand https://orcid.org/0000-0003-4459-8895
Sanjeevikumar Padmanaban https://orcid.org/0000-0003-3212-2750
S. M. Muyeen https://orcid.org/0000-0003-4955-6889

REFERENCES

1. Yang, C., Su, C., Hu, H., Habibi, M., Safarpour, H., Khadimallah, M.A.: Performance optimization of photovoltaic and solar cells via a hybrid and efficient chimp algorithm. Sol. Energy 253, 343–359 (2023)
2. Imani, M.H., Niknejad, P., Barzegaran, M.R.: The impact of customers' participation level and various incentive values on implementing emergency demand response program in microgrid operation. Int. J. Electr. Power Energy Syst. 96, 114–125 (2018)
3. El-Fergany, A.A.: Parameters identification of PV model using improved slime mould optimizer and Lambert W-function. Energy Rep. 7, 875–887 (2021)
4. Haider, R., D'Achiardi, D., Venkataramanan, V., Srivastava, A., Bose, A., Annaswamy, A.M.: Reinventing the utility for distributed energy resources: a proposal for retail electricity markets. Adv. Appl. Energy 2, 100026 (2021)
5. Jha, S.K., Bilalovic, J., Jha, A., Patel, N., Zhang, H.: Renewable energy: present research and future scope of Artificial Intelligence. Renewable Sustainable Energy Rev. 77, 297–317 (2017)
6. Maleki, A., Pourfayaz, F.: Sizing of stand-alone photovoltaic/wind/diesel system with battery and fuel cell storage devices by harmony search algorithm. J. Energy Storage 2, 30–42 (2015)
7. Modu, B., Abdullah, M.P., Bukar, A.L., Hamza, M.F., Adewolu, M.S.: Energy management and capacity planning of photovoltaic-wind-biomass energy system considering hydrogen-battery storage. J. Energy Storage 73, 109294 (2023)
8. Raveendhra, D., Poojitha, R., Narasimharaju, B.L., Dreglea, A., Liu, F., Panasetsky, D., Pathak, M., Sidorov, D.: Part-I: state-of-the-art technologies of solar powered DC microgrid with hybrid energy storage systems-architecture topologies. Energies 16(2), 923 (2023)
9. Mahmoodzadeh, A., Mohammadi, M., Noori, K.M.G., Khishe, M., Ibrahim, H.H., Ali, H.F.H., Abdulhamid, S.N.: Presenting the best prediction model of water inflow into drill and blast tunnels among several machine learning techniques. Autom. Constr. 127, 103719 (2021)
10. Ebrahimi, S.M., Salahshour, E., Malekzadeh, M., Gordillo, F.: Parameters identification of PV solar cells and modules using flexible particle swarm optimization algorithm. Energy 179, 358–372 (2019)
11. El-Dabah, M.A., El-Sehiemy, R.A., Hasanien, H.M., Saad, B.: Photovoltaic model parameters identification using Northern Goshawk optimization algorithm. Energy 262, 125522 (2023)
12. Xiong, G., Zhang, J., Yuan, X., Shi, D., He, Y., Yao, G.: Parameter extraction of solar photovoltaic models by means of a hybrid differential evolution with whale optimization algorithm. Sol. Energy 176, 742–761 (2018)
13. Elshahed, M., El-Rifaie, A.M., Tolba, M.A., Ginidi, A., Shaheen, A., Mohamed, S.A.: An innovative hunter-prey-based optimization for electrically based single-, double-, and triple-diode models of solar photovoltaic systems. Mathematics 10(23), 4625 (2022)
14. Chenouard, R., El-Sehiemy, R.A.: An interval branch and bound global optimization algorithm for parameter estimation of three photovoltaic models. Energy Convers. Manage. 205, 112400 (2020)
15. Yaghoubi, M., Eslami, M., Noroozi, M., Mohammadi, H., Kamari, O., Palani, S.: Modified SALP swarm optimization for parameter estimation of solar PV models. IEEE Access 10, 110181–110194 (2022)
16. Ibrahim, I.A., Hossain, M.J., Duck, B.C., Nadarajah, M.: An improved wind driven optimization algorithm for parameters identification of a triple-diode photovoltaic cell model. Energy Convers. Manage. 213, 112872 (2020)
17. Olabi, A.G., Rezk, H., Abdelkareem, M.A., Awotwe, T., Maghrabie, H.M., Selim, F.F., Rahman, S.M.A., Shah, S.K., Zaky, A.A.: Optimal parameter identification of perovskite solar cells using modified bald eagle search optimization algorithm. Energies 16(1), 471 (2023)
18. Alghamdi, M.A., Khan, M.F.N., Khan, A.K., Khan, I., Ahmed, A., Kiani, A.T., Khan, M.A.: PV model parameter estimation using modified FPA with dynamic switch probability and step size function. IEEE Access 9, 42027–42044 (2021)
19. Ye, X., Liu, W., Li, H., Wang, M., Chi, C., Liang, G., Chen, H., Huang, H.: Modified whale optimization algorithm for solar cell and PV module parameter identification. Complexity 2021, 1–23 (2021)
20. Aldosary, A., Ali, Z.M., Alhaider, M.M., Ghahremani, M., Dadfar, S., Suzuki, K.: A modified shuffled frog algorithm to improve MPPT controller in PV System with storage batteries under variable atmospheric conditions. Control Eng. Pract. 112, 104831 (2021)
21. Yang, C., Nutakki, T.U.K., Alghassab, M.A., Alkhalaf, S., Alturise, F., Alharbi, F.S., Elmasry, Y., Abdullaev, S.: Optimized integration of solar energy and liquefied natural gas regasification for sustainable urban development: dynamic modeling, data-driven optimization, and case study. J. Cleaner Prod. 447, 141405 (2024)
22. Ma, Z., Zhao, J., Yu, L., Yan, M., Liang, L., Wu, X., Xu, M., Wang, W., Yan, S.: A review of energy supply for biomachine hybrid robots. Cyborg Bionic Syst. 4, 0053 (2023)
23. Zhang, J., Zhong, A., Huang, G., Yang, M., Li, D., Teng, M., Han, D.: Enhanced efficiency with CDCA co-adsorption for dye-sensitized solar cells based on metallosalophen complexes. Sol. Energy 209, 316–324 (2020)
24. Zhu, C.: Optimizing and using AI to study of the cross-section of finned tubes for nanofluid-conveying in solar panel cooling with phase change materials. Eng. Anal. Boundary Elem. 157, 71–81 (2023)
25. Zhu, C., Wang, M., Guo, M., Deng, J., Du, Q., Wei, W., Zhang, Y., Talesh, S.S.A.: Optimizing solar-driven multi-generation systems: a cascade heat recovery approach for power, cooling, and freshwater production. Appl. Therm. Eng. 240, 122214 (2024)
26. Zheng, S., Hai, Q., Zhou, X., Stanford, R.J.: A novel multi-generation system for sustainable power, heating, cooling, freshwater, and methane production: thermodynamic, economic, and environmental analysis. Energy 290, 130084 (2024)
27. Zhu, C., Wang, M., Guo, M., Deng, J., Du, Q., Wei, W., Zhang, Y., Mohebbi, A.: An innovative process design and multi-criteria study/optimization of a biomass digestion-supercritical carbon dioxide scenario toward boosting a geothermal-driven cogeneration system for power and heat. Energy 292, 130408 (2024)
28. Wang, Y., Xu, J., Qiao, L., Zhang, Y., Bai, J.: Improved amplification factor transport transition model for transonic boundary layers. AIAA J. 61(9), 3866–3882 (2023)

29. Bai, X., Xu, M., Li, Q., Yu, L.: Trajectory-battery integrated design and its application to orbital maneuvers with electric pump-fed engines. Adv. Space Res. 70(3), 825–841 (2022)
30. Ebrahimi, S.M., Norouzi, F., Dastres, H., Faieghi, R., Naderi, M., Malekzadeh, M.: Sensor fault detection and compensation with performance prescription for robotic manipulators. J. Franklin Inst. 361(7), 106742 (2024)
31. Saadaoui, D., Elyaqouti, M., Assalaou, K., Lidaighbi, S.: Parameters optimization of solar PV cell/module using genetic algorithm based on non-uniform mutation. Energy Convers. Manage.: X 12, 100129 (2021)
32. Qais, M.H., Hasanien, H.M., Alghuwainem, S.: Transient search optimization for electrical parameters estimation of photovoltaic module based on datasheet values. Energy Convers. Manage. 214, 112904 (2020)
33. Oliva, D., Cuevas, E., Pajares, G.: Parameter identification of solar cells using artificial bee colony optimization. Energy 72, 93–102 (2014)
34. Yang, B., Wang, J., Zhang, X., Yu, T., Yao, W., Shu, H., Zeng, F., Sun, L.: Comprehensive overview of meta-heuristic algorithm applications on PV cell parameter identification. Energy Convers. Manage. 208, 112595 (2020)
35. Pourmousa, N., Ebrahimi, S.M., Malekzadeh, M., Alizadeh, M.: Parameter estimation of photovoltaic cells using improved Lozi map based chaotic optimization Algorithm. Sol. Energy 180, 180–191 (2019)
36. Norouzi, S., et al.: Stability analysis of variable frequency control method of soft switching for boost converter with wide bandgap semiconductors. In: 2023 14th Power Electronics, Drive Systems, and Technologies Conference (PEDSTC), pp. 1–7. IEEE, Piscataway, NJ (2023)
37. Yang, X., Gong, W.: Opposition-based JAYA with population reduction for parameter estimation of photovoltaic solar cells and modules. Appl. Soft Comput. 104, 107218 (2021)
38. Yan, Z., Li, C., Song, Z., Xiong, L., Luo, C.: An improved brain storming optimization algorithm for estimating parameters of photovoltaic models. IEEE Access 7, 77629–77641 (2019)
39. El-Dabah, M.A., El-Sehiemy, R.A., Hasanien, H.M., Saad, B.: Photovoltaic model parameters identification using an innovative optimization algorithm. IET Renewable Power Gener. 17(7), 1783–1796 (2023)
40. Naeijian, M., Rahimnejad, A., Ebrahimi, S.M., Pourmousa, N., Gadsden, S.A.: Parameter estimation of PV solar cells and modules using Whippy Harris Hawks optimization algorithm. Energy Rep. 7, 4047–4063 (2021)
41. Ali, E.S., El-Sehiemy, R.A., El-Ela, A.A.A., Kamel, S., Khan, B.: Optimal planning of uncertain renewable energy sources in unbalanced distribution systems by a multi-objective hybrid PSO–SCO algorithm. IET Renewable Power Gener. 16(10), 2111–2124 (2022)
42. Rajasekar, N., Kumar, N.K., Venugopalan, R.: Bacterial foraging algorithm based solar PV parameter estimation. Sol. Energy 97, 255–265 (2013)
43. Abd Elaziz, M., Oliva, D.: Parameter estimation of solar cells diode models by an improved opposition-based whale optimization algorithm. Energy Convers. Manage. 171, 1843–1859 (2018)
44. Elahi, P., Horsley, J., Sparks, T.D.: Electrochemical and degradation studies on one-dimensional tunneled sodium zirconogallate (NZGO)+ yttria-stabilized zirconia (YSZ) composite, mixed sodium and oxygen ion conductor. J. Electrochem. Soc. 169(11), 114502 (2022)
45. Noruzi, S., et al.: Variable frequency control method of boost converter operating in boundary conduction mode. In: 2020 IEEE 61th International Scientific Conference on Power and Electrical Engineering of Riga Technical University (RTUCON). IEEE, Piscataway, NJ (2020)
46. Jamali, B., Rasekh, M., Jamadi, F., Gandomkar, R., Makiabadi, F.: Using PSO-GA algorithm for training artificial neural network to forecast solar space heating system parameters. Appl. Therm. Eng. 147, 647–660 (2019)
47. Jamali, H., et al.: A schedule of duties in the cloud space using a modified SALP swarm algorithm. In: IFIP International Internet of Things Conference. Springer, Cham (2023)
48. Pourmousa, N., Ebrahimi, S.M., Malekzadeh, M., Gordillo, F.: Using a novel optimization algorithm for parameter extraction of photovoltaic cells and modules. Eur. Phys. J. Plus 136(4), 470 (2021)
49. Ebrahimi, S.M., Hasanzadeh, S., Khatibi, S.: Parameter identification of fuel cell using repairable grey wolf optimization algorithm. Appl. Soft Comput. 147, 110791 (2023)
50. Salahshour, E., Malekzadeh, M., Gordillo, F., Ghasemi, J.: Quantum neural network-based intelligent controller design for CSTR using modified particle swarm optimization algorithm. Trans. Inst. Meas. Control 41(2), 392–404 (2019)
51. Salahshour, E., Malekzadeh, M., Gholipour, R., Khorashadizadeh, S.: Designing multi-layer quantum neural network controller for chaos control of rod-type plasma torch system using improved particle swarm optimization. Evol. Syst. 10, 317–331 (2019)
52. Rastegar, S., Araújo, R., Malekzadeh, M., Gomes, A., Jorge, H.: A new NIALM system design based on neural network architecture and adaptive springy particle swarm optimization algorithm. Energy Effic. 16(6), 1–17 (2023)
53. Taleshian, T., Malekzadeh, M., Sadati, J.: Parameters identification of photovoltaic solar cells using FIPSO-SQP algorithm. Optik 283, 170900 (2023)
54. Ebrahimi, S.M., Malekzadeh, M., Alizadeh, M., HosseinNia, S.H.: Parameter identification of nonlinear system using an improved Lozi map based chaotic optimization algorithm (ILCOA). Evol. Syst. 12, 255–272 (2021)
55. Saremi, S., Mirjalili, S., Lewis, A.: Grasshopper optimisation algorithm: theory and application. Adv. Eng. Software 105, 30–47 (2017)
56. Ho, M.M., et al.: DISC: latent diffusion models with self-distillation from separated conditions for prostate cancer grading. arXiv:2404.13097 (2024)
57. Yu, K., Qu, B., Yue, C., Ge, S., Chen, X., Liang, J.: A performance-guided JAYA algorithm for parameters identification of photovoltaic cell and module. Appl. Energy 237, 241–257 (2019)
58. Deshpande, A., et al.: Automatic light intensity modulation using TNC-based artificial iris for smart contact lens. In: *2023 IEEE SENSORS*, pp. 1–4. IEEE, Piscataway, NJ (2023)
59. Chaibi, Y., Salhi, M., El-Jouni, A., Essadki, A.: A new method to extract the equivalent circuit parameters of a photovoltaic panel. Sol. Energy 163, 376–386 (2018)
60. Ferrero, A., et al.: HistoEM: a pathologist-guided and explainable workflow using histogram embedding for gland classification. Mod. Pathol. 37(4), 100447 (2024)
61. Ghosh, C., et al.: Artificial iris on smart contact lens using twisted nematic cell for photophobia alleviation. In: 2023 IEEE Photonics Conference (IPC), pp. 1–2. IEEE, Piscataway, NJ (2023)
62. Chen, X., Xu, B., Mei, C., Ding, Y., Li, K.: Teaching–learning–based artificial bee colony for solar photovoltaic parameter estimation. Appl. Energy 212, 1578–1588 (2018)
63. Moon, H., et al.: The influence of olfactory and visual stimuli on students' performance and mood in virtual reality environment. In: Proceedings of the Human Factors and Ergonomics Society Annual Meeting, vol. 67, pp. 2441–2446. Sage Publications, Thousand Oaks, CA (2023)
64. Chen, X., Tianfield, H., Mei, C., Du, W., Liu, G.: Biogeography-based learning particle swarm optimization. Soft Comput. 21, 7519–7541 (2017)

How to cite this article: Jabari, M., Rad, A., Nasab, M.A., Zand, M., Padmanaban, S., Muyeen, S.M., Guerrero, J.M.: Parameter identification of PV solar cells and modules using bio dynamics grasshopper optimization algorithm. IET Gener. Transm. Distrib. 18, 3314–3338 (2024). https://doi.org/10.1049/gtd2.13279